Applied Catalysis B: Environmental 191 (2016) 209–227

Contents lists available at ScienceDirect

Applied Catalysis B: Environmental

journal homepage: www.elsevier.com/locate/apcatb

Waste chicken eggshell as a natural valuable resource and environmentally benign support for biosynthesis of catalytically active Cu/eggshell, Fe_3O_4/eggshell and Cu/Fe_3O_4/eggshell nanocomposites

Mahmoud Nasrollahzadeh [a,b,*], S. Mohammad Sajadi [c], Arezo Hatamifard [a]

[a] Department of Chemistry, Faculty of Science, University of Qom, Qom 37185-359, Iran
[b] Center of Environmental Researches, University of Qom, Qom, Iran
[c] Department of Petroleum Geoscience, Faculty of Science, Soran University, P.O. Box 624, Soran, Kurdistan Regional Government, Iraq

ARTICLE INFO

Article history:
Received 20 December 2015
Received in revised form 1 February 2016
Accepted 16 February 2016
Available online 15 March 2016

Keywords:
Eggshell
Orchis mascula L.
$NaBH_4$
Organic dyes
Water

ABSTRACT

This paper is reported on the green synthesis of Cu/eggshell, Fe_3O_4/eggshell and Cu/Fe_3O_4/eggshell nanocomposites through an environmental and economical method using aqueous extract of the leaves of *Orchis mascula* L. without any stabilizer or surfactant. The nanocomposites showed high catalytic activity in the reduction of a variety of dyes and characterized by Fourier transform infrared spectroscopy (FT-IR), differential thermal and thermogravimetric (DTA-TGA) analysis, field emission scanning electron microscopy (FESEM) equipped with an energy dispersive spectroscopy (EDS), elemental mapping, X-ray diffraction analysis (XRD), Brunauer–Emmett–Teller (BET), vibrating sample magnetometer (VSM) and UV–vis spectroscopy. The possible mechanism leading to the formation of copper nanoparticles (NPs) is also suggested. The facile and clean synthesis, simple preparation procedure, excellent properties, alterable supports and low cost allow these catalysts to be used in reduction of 4-nitrophenol (4-NP), Methyl orange (MO), Congo red (CR), Methylene blue (MB) and Rhodamine B (RhB) in water at room temperature. The progress of the reaction was monitored using UV–vis spectroscopy. The catalysts could be easily removed from the reaction media by mild centrifugation or an external magnet and reused several times without any negative effect on the initial results.

1. Introduction

Most effluents usually contain important quantities of synthetic organic dyes which the discharge of these colored compounds in the environment causes considerable pollutions and serious health-risk factors. Since conventional wastewater treatment plants cannot degrade the majority of these pollutants, powerful methods for the decontamination of dyes wastewaters have received increasing attention over the past decade. Therefore, efficient catalytic reduction of toxic organic pollutants from wastewater has become a hot research topic due to its ecological and environmental importance [1].

Nanomaterials such as nanoparticles are being used for several applications in catalytic, chemical and biological fields due to their unique characteristics [2–5]. Among various metal nanoparticles, copper nanoparticles (NPs) can be used in different fields because of their catalytic, optical, and electrical conducting properties [6]. There are several methods for the preparation of copper NPs, including thermal reduction, metal vapor synthesis, radiation methods, microemulsion techniques, laser ablation, mechanical attrition, and chemical reduction [7–14].

Most of the preparation methods have some disadvantages such as environmentally unpleasant use of organic solvents, expensive, toxic and hazardous reagents, low purity, the use of complicated equipments, wide particle size distribution, harsh reaction conditions and formation of side products. In addition, the need for toxic solvents and the contamination from chemicals used in the preparation of nanoparticles limit their potential use in biomedical applications. Therefore, it is desirable to develop more efficient, convenient, non-toxic and 'greener' methods for the synthesis of metallic nanoparticles under mild conditions with avoiding organic solvents and toxic reagents.

* Corresponding author at: Department of Chemistry, Faculty of Science, University of Qom, Qom 37185-359, Iran.
E-mail address: mahmoudnasr81@gmail.com (M. Nasrollahzadeh).

http://dx.doi.org/10.1016/j.apcatb.2016.02.042
0926-3373/

In recent years, biosynthesis of metallic nanoparticles using environmentally benign materials like gum or plant extract [15–18] has been received increasing attention due to a growing need to develop green technologies in material synthesis. Among these methods, the usage of plants for NPs synthesis is more simple, faster, reliable and cost effective over other biological processes and the most versatile for special variety of nanosized particles especially copper and magnetite NPs. In fact during the past decade, the synthesis of magnetite nanoparticles has been intensively developed for fundamental scientific interest and technological applications such as magnetic storage media, biosensing applications, its excellent catalytic activity in chemical reactions, medical applications and magnetic inks for jet printing. Beside the significant applications of magnetite NPs in science and technology, the stabilization and stability characteristics of magnetic colloidal suspension which results from the equilibrium between attractive and repulsive forces such as resistance against deformation and decomposition processes and also aggregation in both a biological medium and a magnetic field is crucial [5].

In the field of catalysis, Cu NPs play an important role in the overall catalytic performance [6]. However, Cu NPs have some drawbacks such as difficulties in quantitative separation from the reaction mixture and the impossibility to reuse it in consecutive reactions, the over-stoichiometric use of Cu reagents and their agglomeration [19]. In order to solve the above problems, recently, Cu NPs were immobilized on/into solid supports such as zeolite, magnetic-materials and graphene to form composite catalysts [2,3,19–21]. Our recent study has shown that the natural Natrolite zeolite can be used as a very active support in the immobilization of metal NPs [21]. Natural Natrolite zeolite is a good support, but there are difficulties in its preparation and availability. Therefore, it is highly desirable to develop a facile method to fabricate Cu NPs with well dispersion and stability and their immobilization on an effective support. An alternative method of immobilization is the use of bio-derived materials as environmentally benign supports.

In recent years, there has been a tremendous upsurge of interest in the application of biowaste materials such as eggshell waste. Low-cost eggshell waste has been used widely as a possible bone substitute, catalyst, support, inexpensive adsorbent for removal of ionic pollutant and dyes from the aqueous medium, coating pigments for inkjet printing paper, the starting material for preparing calcium phosphate bioceramics (*e.g.* hydroxyapatite) and efficient bio-templates in recent years due to their high catalytic activity, ease of handling, reusability and benign character [22–37]. The eggshell is a cheap and easily available biomaterial and has intrinsic pore structure. According to the literature, the chemical composition of eggshell is calcium carbonate (94%), magnesium carbonate (1%), calcium phosphate (1%) and organic matter (4%) [22]. It is particularly attractive for synthesizing metal nanoparticles because strong metal-protein bonding can be readily utilized [22–37]. The application of waste eggshell as a support not only provides a cost-effective and environmental friendly way for the heterogeneous catalysts production, but also makes the process of economic and fully ecologically friendly heterogeneous catalysts production. Recently, waste eggshell have been used as a catalyst for biodiesel synthesis, lactose isomerization and preparation of dimethyl carbonate [35–37]. However, to the best of our knowledge, *in situ* biosynthesis of metallic NPs supported on the eggshell surface using plant extracts is not reported to date.

Orchis mascula L. locally known as Saalab misri, from the family of *Orchidaceae* (Fig. 1) is found in most parts of Europe and North Africa, as well as in Western and Northern Asia specially Iran and Afghanistan and used for medicinal purposes for nervous and muscular, as well as sexual dysfunctions and cardiovascular diseases, alleviating diarrhea, dysentery and chronic inflammation [38–40]. Furthermore, through the current study on the phytochemical screening of the crude extract of ground powder of *Orchis mascula* L. the presence of alkaloids, saponins, tannins, terpenes, sterols and antioxidant phenolics and flavonoids were demonstrated [41–44]. These phyto-constituents confirmed the application of *Orchis mascula* L. leaf extract as a suitable source for the synthesis of Cu NPs using the reducing ability of these potent antioxidants. Compared with the other literature works on the synthesis of NPs, the notable features of our method are: (i) Our source was plant as a green source; (ii) The mechanism of synthesized NPs is according the bioactivity of natural source; (iii) Phytochemicals responsible for this synthesis were taken from a green source; (iv) In this study the reducing effect of antioxidant content of the plant caused to the synthesis of NPs not anything else; (v) On the other hand, these environmentally benign and safe protocols have advantages such as simple equipment, short process, very mild reaction conditions, use of nontoxic solvents such as water, elimination of toxic and dangerous materials and cost effectiveness as well as compatibility for biomedical and pharmaceutical applications and easy industrial production.

Fig. 1. Image of *Orchis mascula* L.

In continuation of our efforts to develop environmentally friendly synthetic methodologies [45–47], in the current work for the first time, a facile one-step and green route has been applied for the biosynthesis of Cu/eggshell, Fe_3O_4/eggshell and Cu/Fe_3O_4/eggshell nanocomposites from waste chicken eggshell using aqueous extract of the leaves of *Orchis mascula* L. as a stabilizing and reducing agent. The presented synthesis procedure is simple, green, environment friendly, economical, non-toxic, and free of the use of any organic solvents, surfactants and specialized instruments. The nanocomposites were utilized for reduction of 4-NP, MO, CR, MB and RhB in water at room temperature. The facile synthesis, excellent properties, alterable supports and low cost allow these nanocomposites to be used in the reduction of a variety of dyes.

2. Experimental

2.1. Instruments and reagents

High-purity chemical reagents were purchased from the Merck and Aldrich chemical companies. All materials were of commercial reagent grade. Eggs from hens were purchased from a local supermarket. Egg yolk and white were manually separated prior to use. FT-IR spectra were recorded on a Nicolet 370 FT/IR spectrometer (Thermo Nicolet, USA) using pressed KBr pellets. The natural zeolite used in this study originated from Hormak area, Iran. X-ray diffraction (XRD) measurements were carried out using a Philips powder diffractometer type PW 1373 goniometer (CuKα = 1.5406 A°). The scanning rate was 2°/min in the 2θ range from 10 to 80°. Scanning electron microscopy (SEM) was performed on a Cam scan MV2300. EDS (S3700N) was utilized for chemical analysis of prepared nanos-

tructures. Thermogravimetric-differential thermal analysis was performed using STA 1500 Rheometric Scientific (England). The flow rate of air was 120 mL/min and the ramping rate of sample was 2 °C/min. The UV–vis measurements were performed at room temperature by a PerkinElmer 550ES from 300 to 800 nm with a resolution of 1 nm. The Brunauer–Emmett–Teller (BET) specific surface areas (SBET) and the porosity of the samples were evaluated on the basis of nitrogen adsorption isotherms measured at 77 K using a BELSORP-max nitrogen adsorption apparatus (Japan Inc.). VSM (Vibrating sample magnetometer) measurements were performed by using a SQUID magnetometer at 298 K (Quantum Design MPMS XL). The shape and size of nanocomposites were identified by transmission electron microscope (TEM) using a Philips EM208 microscope operating at an accelerating voltage of 90 kV.

2.2. Preparation of extract of the leaves of Orchis mascula L.

50 g of dried leaf powdered of *Orchis mascula* L. was added to 250 mL double distillated water in 500 mL flask and well mixed. The preparation of extract was done by using magnetic heating stirrer at 70 °C for 30 min. The obtained extract was centrifuged in 7000 rpm and filtered then filtrate was kept at refrigerator to use further.

2.3. Green synthesis of copper nanoparticles using Orchis mascula L. leaf extract

In a 250 mL conical flask, 10 mL solution of $CuCl_2{\cdot}2H_2O$ (5 mM) was mixed with 100 mL of the aqueous plant extract (100 g dried leaf of the plant extracted using 500 mL of deionized water while heating at 80 °C and pH 9 for 30 min then filtered) along with vigorous shaking until gradually changing the color of the mixture during 20 min to dark indicating the formation of Cu nanoparticles (as monitored by UV–vis and FT-IR spectra of the solution). The well shaked mixture then filtered and centrifuged at 6500 rpm for 30 min and obtained precipitation washed with absolute ethanol and double distillated water, respectively.

2.4. Preparation of Cu/eggshell nanocomposite

In a 100 mL conical flask, after pretreatment of eggshells, 1.0 g dried powdered eggshell was mixed with 0.4 g $CuCl_2{\cdot}2H_2O$ and 50 mL of the aqueous plant extract then heated at 70 °C while vigorous shaking for 3 h until gradually changing the color of the mixture indicating the formation of Cu/eggshell nanocomposite then filtered (as monitored by UV–vis).

2.5. Preparation of Fe_3O_4/eggshell nanocomposite

In a 100 mL conical flask, after pretreatment of eggshells, 1.0 g dried powdered eggshell was mixed with 0.5 g $FeCl_3{\cdot}6H_2O$ and 50 mL of the aqueous plant extract in an alkaline media adjusted using 1.0 M Na_2CO_3 then heated at 70 °C while vigorous shaking for 3 h until gradually changing the color of the mixture indicating the formation of Fe_3O_4/Eggshell nanocomposite then filtered (as monitored by UV–vis).

2.6. Preparation of Cu/Fe_3O_4/eggshell nanocomposite

In a 250 mL conical flask, after pretreatment of eggshells, 1.0 g dried powdered eggshell was mixed with 100 mL of the aqueous plant extract. In next step 0.5 g aqueous solution of $FeCl_3{\cdot}6H_2O$ and 0.2 g aqueous solution of $CuCl_2{\cdot}2H_2O$ were added dropwise in an alkaline media adjusted using 1.0 M Na_2CO_3 while stirring then the mixture heated at 70 °C for 3 h until gradually changing the color of the mixture which indicates the formation of Cu/Fe_3O_4/Eggshell nanocomposite and then filtered.

2.7. 4-NP catalytic reduction

In a typical experiment, 5.0 mg of the Cu/eggshell (7.0 mg in case of Fe_3O_4/eggshell and Cu/Fe_3O_4/eggshell) was added to an aqueous solution that contained 4-nitrophenol (2.5 mM, 25 mL), freshly prepared aqueous $NaBH_4$ solution (250 mM, 25 mL) and stirred for 100 s (300 s and 250 s in case of Fe_3O_4/eggshell and Cu/Fe_3O_4/eggshell) at room temperature. The rate of 4-nitrophenol reduction was evaluated using UV–vis spectroscopy at room temperature. After completion of the reaction, the catalyst was separated from the reaction mixture by centrifugation (with an external magnet in case of Fe_3O_4/eggshell and Cu/Fe_3O_4/eggshell), washed with doubly distilled water and then dried for the next cycle.

2.8. MO catalytic reduction

In a typical experiment, 7.0 mg of the Cu/eggshell (Fe_3O_4/eggshell or Cu/Fe_3O_4/eggshell) was added to an aqueous solution that contained MO (3.0×10^{-5} M, 25 mL), freshly prepared aqueous $NaBH_4$ solution (5.3×10^{-3} M, 25 mL) and stirred for 2 min (13 min and 12:14 min in case of Fe_3O_4/eggshell and Cu/Fe_3O_4/eggshell) at room temperature. The change of the absorption peak at 465 nm was recorded to reflect the successive information about the reduction of MO. After completion of the reaction, the catalyst was separated from the reaction mixture by centrifugation (with an external magnet in case of Fe_3O_4/eggshell and Cu/Fe_3O_4/eggshell), washed with doubly distilled water and then dried for the next cycle.

2.9. MB catalytic reduction

In a typical experiment, 3.0 mg of the Cu/eggshell (10.0 mg in case of Cu/Fe_3O_4/eggshell) was added to an aqueous solution that contained MB (3.1×10^{-5} M, 25 mL), freshly prepared aqueous $NaBH_4$ solution (5.3×10^{-3} M, 25 mL) and stirred for 10 s (34 s in case of Cu/Fe_3O_4/eggshell) at room temperature. The change of the absorption peak at 663 nm was recorded to reflect the successive information about the reduction of MB. After completion of the reaction, the catalyst was separated from the reaction mixture by centrifugation (with an external magnet in case of Cu/Fe_3O_4/eggshell), washed with doubly distilled water and then dried for the next cycle.

2.10. RhB catalytic reduction

In a typical experiment, 10.0 mg of the Cu/eggshell was added to an aqueous solution that contained RhB (2.09×10^{-5} M, 25 mL), freshly prepared aqueous $NaBH_4$ solution (5.3×10^{-3} M, 25 mL) and stirred for 90 s at room temperature. The change of the absorption peak at 554 nm was recorded to reflect the successive information about the reduction of RhB. After completion of the reaction, the catalyst was separated from the reaction mixture by centrifugation, washed with doubly distilled water and then dried for the next cycle.

2.11. CR catalytic reduction

In a typical experiment, 7.0 mg of the catalyst was added to an aqueous solution that contained CR (1.44×10^{-5} M, 25 mL), freshly prepared aqueous $NaBH_4$ solution (5.3×10^{-3} M, 25 mL) and stirred for 65 s (116 s and 130 s in case of Fe_3O_4/eggshell and Cu/Fe_3O_4/eggshell) at room temperature. The change of the

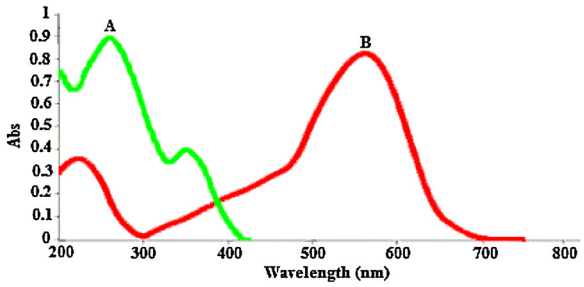

Fig. 2. UV–vis spectrum of the aqueous extract of the leaves of *Orchis mascula* L. (A) and green synthesized Cu NPs (B).

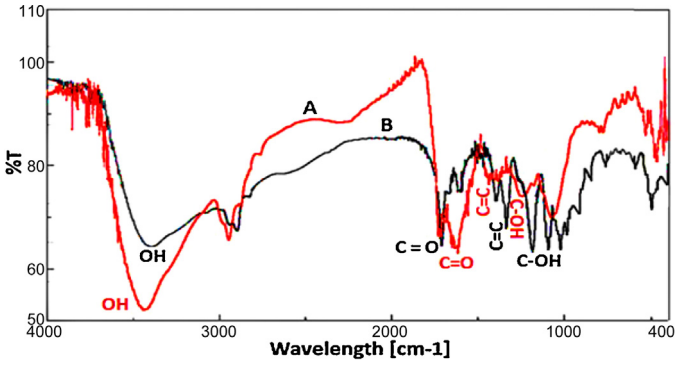

Fig. 3. FT-IR spectrum of the aqueous extract of the leaves of *Orchis mascula* L. (A) and green synthesized Cu NPs (B).

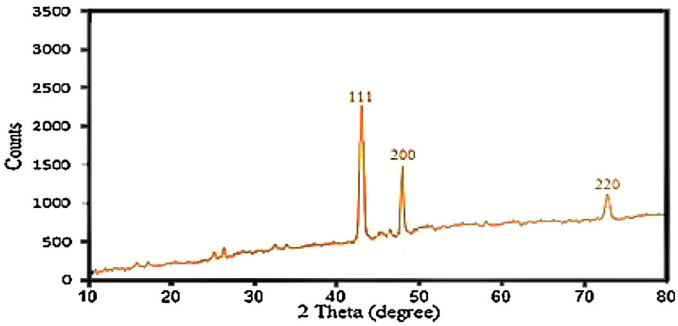

Fig. 4. XRD powder pattern of Cu NPs synthesized using aqueous extract of the leaves of *Orchis mascula* L.

absorption peak at 493 nm was recorded to reflect the successive information about the reduction of CR. After completion of the reaction, the catalyst was separated from the reaction mixture by centrifugation (with an external magnet in case of Fe_3O_4/eggshell and Cu/Fe_3O_4/eggshell), washed with doubly distilled water and then dried for the next cycle.

3. Results and discussion

3.1. Preparation of Cu NPs using aqueous extract of the leaves of Orchis mascula L.

Various plant extracts can be used for the reduction as well as capping of the NPs [15–18]. With these evidences, in this work we investigated the facile and stable green synthesis of Cu NPs by the reduction of Cu^{2+} ions using aqueous extract of the leaves of *Orchis mascula* L. which were further characterized using UV–vis spectroscopy and FT-IR. The methodology which we have adopted was totally hazard free, clean, non-toxic and environment friendly.

The high phenolic content of the aqueous extract of the leaves of *Orchis mascula* L. possesses strong antioxidant properties, which helped in the reduction of metal ions to nano zero valent (NZV) metallic particles. The formation of Cu NPs with flavonoid and phenolics acids present in the extract of the leaves of *Orchis mascula* L. takes place *via* the following steps: (1) complexation with copper metal salts, (2) simultaneous reduction of copper metal, and (3) capping with oxidized polyphenols/caffeine.

The UV–vis spectroscopy technique and FT-IR analysis were used for the characterization of the extract and the resulting nanoparticles.

The UV spectrum of extract (Fig. 2(A) shows bonds at λ_{max} 337 nm (bond I) due to the transition localized within the ring of cinnamoyl system; whereas the $\pi \rightarrow \pi^*$ transition is shown by double bonds. The extract of *Orchis mascula* L. leaves was obtained in aqueous media to extract highly polar phytochemicals like phenolics with conjugated double bonds (in A, B and C ring of the flavone nuclei) as major *phyto* constituents. Then according the literatures about the plant our result supports this idea [42]. Therefore, the absorption at 262 nm (bond II) is for absorbance of ring related to the benzoyl system and $\pi \rightarrow \pi^*$ transitions and demonstrates the presence of phenolics. Therefore, as shown by spectrum, these signals are finger print characteristic and specification of flavones nuclei inside the extract as reported in literature [44].

The UV–vis spectrum of green synthesized Cu NPs using *Orchis mascula* L. leaf extract (Fig. 2B) showed the significant changes in the absorbance maxima due to the surface plasmon resonance demonstrating the formation of Cu NPs. The color of the solution immediately changed into dark with λ_{max} ranging 575 nm indicating the formation of Cu NPs as characterized by UV–vis spectrum.

Furthermore, the FT-IR of Cu NPs shows demonstrative differences in the shape and location of signals indicating the interaction between $CuCl_2{\cdot}2H_2O$ and involved sites of phytochemicals for production of nanoparticles, (Fig. 3B). Changing the location of peaks at 3500–3100, 1725, 1418, 1300 and 1000 cm^{-1} represent the OH functional groups, carbonyl group (C═O), stretching C═C aromatic ring and C—OH stretching vibrations, respectively. Polyphenolics could be adsorbed on the surface of metal nanoparticles, possibly by interaction through π-electrons interaction in the absence of other strong ligating agents.

The crystalline nature of the Cu NPs was confirmed by XRD. Fig. 4 shows XRD pattern of the Cu NPs. The XRD peaks at 43.4° (111), 48.1° (200) and 74.1° (220) were assigned to the Cu NPs (face-centered cubic, JCPDS no. 71-4610) [17]. The particles size can be found by applying Sherrer's equation and the average particles size is found to be 9 nm.

A mechanism for the synthesis of Cu NPs has been shown in Scheme 1. This is in agreement with our previous findings [45–47].

The following analysis was taken to more confirmation and identification of the plant extract:

- 3D HPLC from the hydro-alcoholic extract of the plant;
- RP-HPLC-DAD from the aqueous extract of the plant;
- Total Phenolic Content assay (TPC) from the plant extract;
- Ferric Reduction Antioxidant Power (FRAP) assay of the plant extract;
- TLC fingerprint profile at 254 nm using chemical reagents from the plant extract.

3.2. Total phenolic content of the Orchis mascula L. aqueous extract

The amount of total phenolics in obtained aqueous extracts before and after interaction to obtain NPs at times ranging 10, 15, 20 and 25 min was determined with Folin–Ciocalteu reagent according to the method with slight modification using gallic acid as a standard [17]. Briefly, 1.0 mL of sample solution was added in

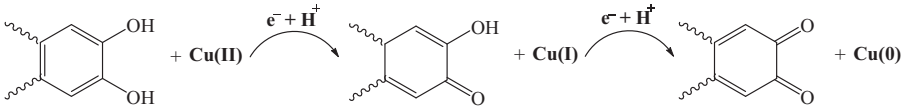

Scheme 1. Mechanism of bioreduction of Cu^{2+} ions to Cu NPs using the aqueous extract of the leaves of *Orchis mascula* L.

a 100 mL volumetric flask containing 60 mL distilled water. Then, 5.0 mL of Folin–Ciocalteu reagent was added and the content of the flask was mixed completely. After 5 min, 15.0 mL Na_2CO_3 (20%) was added and the volume was made up to 100 mL using distilled water. The mixture was allowed to stand for 2 h with shaking then the absorbance was measured at 760 nm. The procedure was repeated in triplicate and total phenolic content determined as mg of gallic acid equivalent (GAE) using an equation obtained from the standard gallic acid calibration graph. The content of phenolics in the plant extracts at different times demonstrated a range of 2500–3300 GAE/dried weight.

3.3. *Total antioxidant ability of the* Orchis mascula *L. aqueous extract*

The amount of antioxidant capacity was determined using FRAP assay [48], which depends upon the reduction of ferric tripyridyltriazine (Fe(III)-TPTZ) complex to the ferrous tripyridyltriazine (Fe(II)-TPTZ) by a reductant at low pH (Fe(II)-TPTZ) has an intensive blue color which can be monitored at 593 nm. Briefly, the stock solutions included 300 mM acetate buffer (3.1 g $C_2H_3NaO_2.3H_2OC_2H_3NaO_2{\cdot}3H_2O$ and 16 mL $C_2H_4O_2$), pH 3.6, 10 mM TPTZ (2,4,6-tripyridyl-s-triazine) solution in 40 mM HCl, and 20 mM $FeCl_3{\cdot}6H_2O$ solution. The fresh working solution was prepared freshly by mixing 25 mL acetate buffer, 2.5 mL TPTZ solution, and 2.5 mL $FeCl_3{\cdot}6H_2O$ solution and then warmed at 37 °C before using. Aqueous solution of known Fe(II) concentration was used as standard solution for calibration (in a range of 0.1–1 mM). Assay: blank FRAP reagent, sample: 1.5 mL FRAP reagent and 50 mL aqueous extracts of the plant. The reaction was monitored up to 4 min at 593 nm, at 37 °C. The Fe(II) standard solution was tested in a parallel process. Calibrations were made by a calibration curve. The standard curve was linear between 1–10 mmol also additional dilution was needed if the FRAP value was over the linear range of the standard curve. The results are expressed in mmol Fe^{+2} per mg sample. Furthermore, the positive antioxidant potential of the *Orchis mascula* L. aqueous extract using FRAP method demonstrated its reducing ability as a suitable source for synthesis of metallic nanoparticles.

3.4. *HPLC analysis of the plant extract*

The RP-HPLC-DAD instrument consisted of auto injector, sample cooler, pumps, and column oven and diode array detector. An ODS 5.0 μm column (250 mm × 4.60 mm, particle size 5.0 μm) was applied. The effluent consisted of a mixture of water-tetrahydrofuran (THF)-trifluoroacetic acid (TFA) (98:2:0.1) (solvent A) and acetonitrile (solvent B). Flow rate of the effluent was 1.0 mL/min, the spectra was recorded using DAD detector from 200 to 400 nm and the volume of injection was 10 μL. Identification was based on co-injections of authentic compounds and comparisons of absorption spectra. All solvents were HPLC-grade and chemicals were analytical grade.

The crude plant extract (200 mg) was dissolved in 2.0 mL 30% acetonitrile to give a 100 mg/mL solution and filtered through 0.2 m membrane filter using high-pressure vacuum pump and the cleared filtrate was injected into HPLC fingerprint analysis.

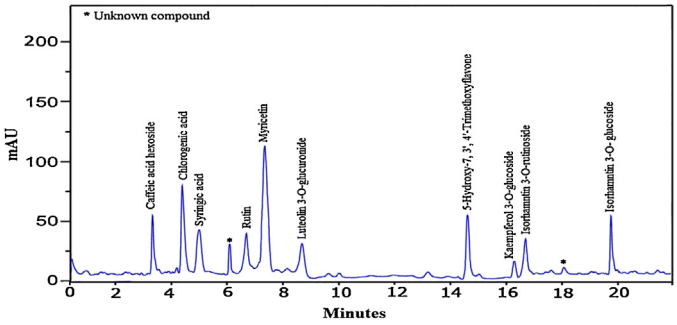

Fig. 5. The RP-HPLC-DAD chromatogram of the aqueous extract of the leaves of *Orchis mascula* L.

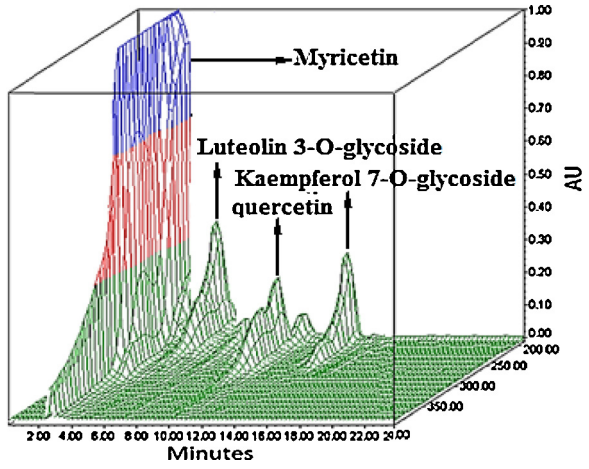

Fig. 6. 3D HPLC-DAD chromatogram of the Hydro alcoholic (EtOH 30%) extract of the leaves of *Orchis mascula* L.; Conditions: column: An ODS 5 μm column (250 mm × 4.60 mm, particle size 5.0 μm), mobile phase: MeOH 30%, Flow rate: 1.0 mL/min, column temperature: 50 °C, detector: PDA scanning from 190 to 400 nm, volume of injection: 10 μL.

Also for further confirmation through our study on phytochemical screening of the *Orchis mascula* L. aqueous and hydroalcoholic extract, RP-HPLC-DAD analysis and TLC fingerprinting using specified reagents, (Figs. 5–7) depicted the presence of phenolic antioxidants and supports the results of literatures [41–44].

3.5. *Preparation of Cu/eggshell nanocomposite*

In a typical synthesis of Cu/eggshell nanocomposite, for further monitoring, first eggshell was characterized by field emission scanning electron microscope (FESEM), energy-dispersive X-ray spectroscopy (EDS) and fourier-transform infrared (FT-IR) spectroscopy.

FESEM images were recorded to understand the morphological changes occurring on the surface of the eggshell. It reveals that the eggshell is a macroporous network (Fig. 8).

The elemental composition of eggshell was also analyzed by EDS spectrum. It further confirmed that eggshell was composed of C, Ca and O (Fig. 9).

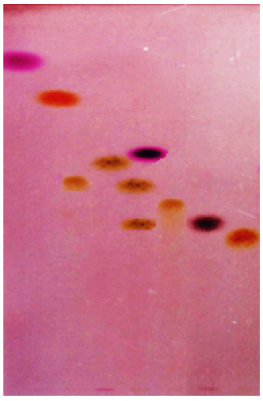

Fig. 7. TLC fingerprint profile of *Orchis mascula* L. aqueous extract; Conditions; Aluminum supported TLC silica gel, Mobile phase: Water: Acetic acid: *n*-Butanol (4:1:1), Detection H_2SO_4 in EtOH.

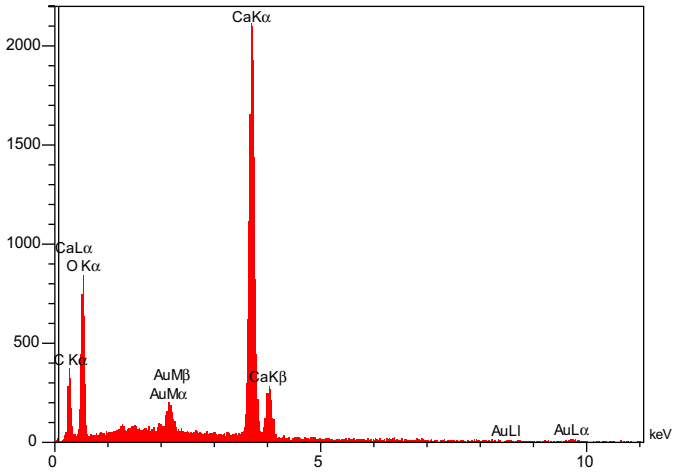

Fig. 9. EDS spectrum of eggshell.

In situ synthesis of Cu NPs supported on eggshell was carried out by simple and green method using aqueous extract of the leaves of *Orchis mascula* L. as the reducing agent as well as stabilizer.

The UV–vis spectra of green Cu/eggshell nanocomposite synthesized using the aqueous extract of the leaves of *Orchis mascula* L. demonstrated the surface plasmon resonance which peak centered at 500 nm indicates the end of the reaction and formation of the product (Fig. 10A).

The elemental composition of Cu/eggshell nanocomposite was analyzed by the Energy Dispersive X-ray Spectroscopy (EDS). This technique further confirmed that Cu/eggshell nanocomposite was composed of Ca, S, Si, Cl, O and Cu (Fig. 11). The amount of Cu incorporated into the Cu/eggshell nanocomposite found to be 11.05 wt%, which determined by EDS.

XRD pattern of Cu/eggshell nanocomposite is shown in Fig. 12. In this Figure, strong and sharp peak at $2\theta = 29.5^\circ$ is the characteristic peak of $CaCO_3$ [49]. The presence of copper was confirmed with powder XRD measurements. The results reveal that Cu loading and thermal treatment did not alter the eggshell structure. The diffraction peaks at 43.4, 48.1 and 73.2 correspond to Cu NPs.

To get the microstructure information of the nanocomposites, the samples were further investigated by field emission scanning electron microscopy (FESEM). Fig. 13 shows the top-view FESEM images of Cu/eggshell nanocomposite. It can easily be seen in Figs. 8 and 13 that the presence of Cu NPs has caused changes in the roughness of the surface. It is clearly observed that the Cu NPs were immobilized on the support surface, which displays a good combination between eggshell and Cu NPs.

Fig. 14 shows TEM images of Cu/eggshell nanocomposite. The Cu NPs were very small with a narrow size distribution. The TEM micrographs show that the Cu NPs are spherical with an average diameter of about 5 nm.

3.6. Preparation of magnetic Fe_3O_4/eggshell nanocomposite

To overcome the separation technicality issue, in this study magnetic eggshell was prepared using a simple method and used as a heterogeneous catalyst in reduction of variety of dyes. The magnetic Fe_3O_4/eggshell was synthesized successfully by a green method using aqueous extract of the leaves of *Orchis mascula* L. without any stabilizer or surfactant.

The UV–vis spectra of green Fe_3O_4/eggshell nanocomposite synthesized using the aqueous extract of *Orchis mascula* L. demonstrated the surface plasmon resonance which peak centered at

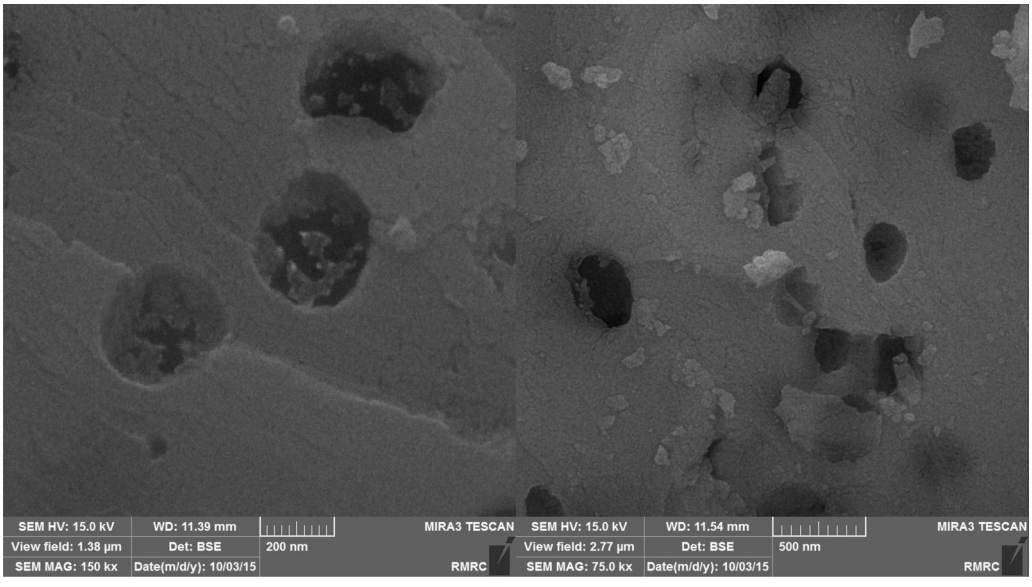

Fig. 8. FESEM images of eggshell.

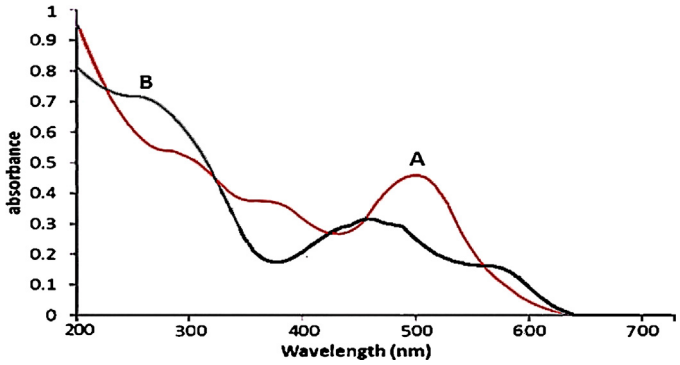

Fig. 10. UV–vis spectrum of green synthesized Cu/eggshell nanocomposite (A) and green synthesized Fe_3O_4/eggshell nanocomposite (B).

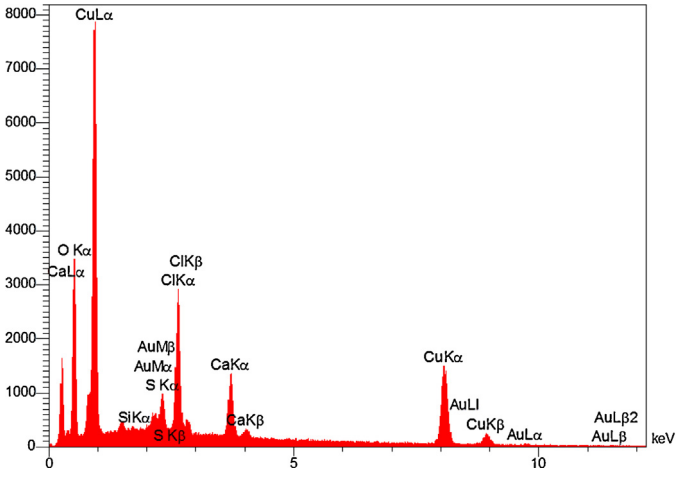

Fig. 11. EDS spectrum of Cu/eggshell nanocomposite.

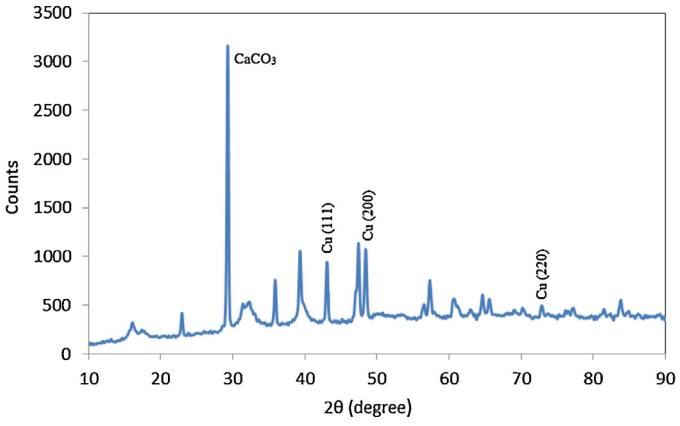

Fig. 12. XRD powder pattern of Cu/eggshell nanocomposite.

470 nm indicates the end of the reaction and formation of product (Fig. 10B).

As indicated, there are antioxidant compounds inside the plant extract therefore based on the proposed mechanism Fe(III) are reduced to Fe(0) then because of the highly oxidation potential of Fe(0) to combination with oxygen and reach the higher oxidation states it spontaneously converts to the Fe_3O_4 NPs, Scheme 2, steps 1 and 2.

The structure and morphology of magnetic Fe_3O_4/eggshell were analyzed by XRD and SEM. Fig. 15 shows a typical XRD pattern of the Fe_3O_4/eggshell especially a peak at $2\theta = 29.5^\circ$ correspond to $CaCO_3$ [49]. Further, five diffraction peaks at $2\theta = 36.1^\circ$, 43.7°, 54.6°, 58.1°

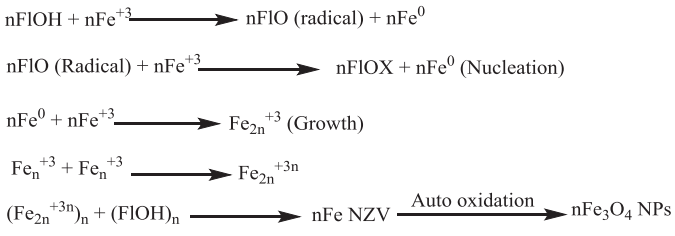

Scheme 2. Reducing ability of antioxidant phenolics of *Orchis mascula* Linn leaf extract to produce nano Fe_3O_4.

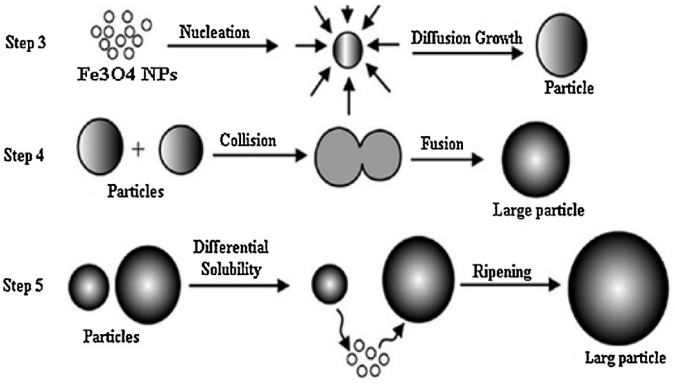

Scheme 3. Formation of Fe_3O_4 nanocrystals using the coagulation of smaller particles to produce the large nanocrystals through quasi-spherical particles as transition state.

and 61.4° appear in the XRD pattern of the Fe_3O_4/eggshell, which can be assigned to the diffraction of (311), (400), (422), (511) and (440) planes of the cubic Fe_3O_4, confirming the formation of the Fe_3O_4.

The FESEM images of magnetic Fe_3O_4/eggshell are shown in Fig. 16. The average size of Fe_3O_4 NPs determined from Fig. 16 was under 22 nm. As shown in Figs. 8, 13 and 16, the eggshell powder particles consist of highly porous structure, which increased the contact area and was responsible for Fe_3O_4 and copper loading onto eggshell powder particles.

The elemental composition of Fe_3O_4/eggshell nanocomposite was also analyzed by EDS spectrum. It further confirmed that Fe_3O_4/eggshell nanocomposite was composed of S, C, Ca, O and Fe (Fig. 17). The amount of Fe incorporated into the Fe_3O_4/eggshell nanocomposite found to be 24.69 wt%, which determined by EDS.

TEM analysis was performed to examine the size and shape of Fe_3O_4/eggshell nanocomposite. Fig. 18 shows TEM images of Fe_3O_4/eggshell nanocomposite. The Fe_3O_4 NPs were very small with sizes of <8 nm.

As demonstrated using X-ray diffraction analysis, the produced Fe_3O_4 NPs has a crystal structure which the formation of these nanocrystals can be explained via the mechanism briefly as formation of Fe_3O_4 nanocrystals using the coagulation of smaller particles to produce the large nanocrystals through quasi-spherical particles as transition state, Scheme 3. Firstly, the produced Fe_3O_4 NPs undergoes nucleation from a required critical number of nanoparticles in the solvent. Step 3 indicates the growth of this nucleus by diffusion process onto the surface of the nucleated particle cause to produce interparticles; in step 4, interparticles growth by collision and fusion of two particles via the oriented attachment route; and in final step interparticles growth via exchange (dissolution and diffusion) of molecules between various particles, commonly referred to ripening of Fe_3O_4 nanocrystals [50].

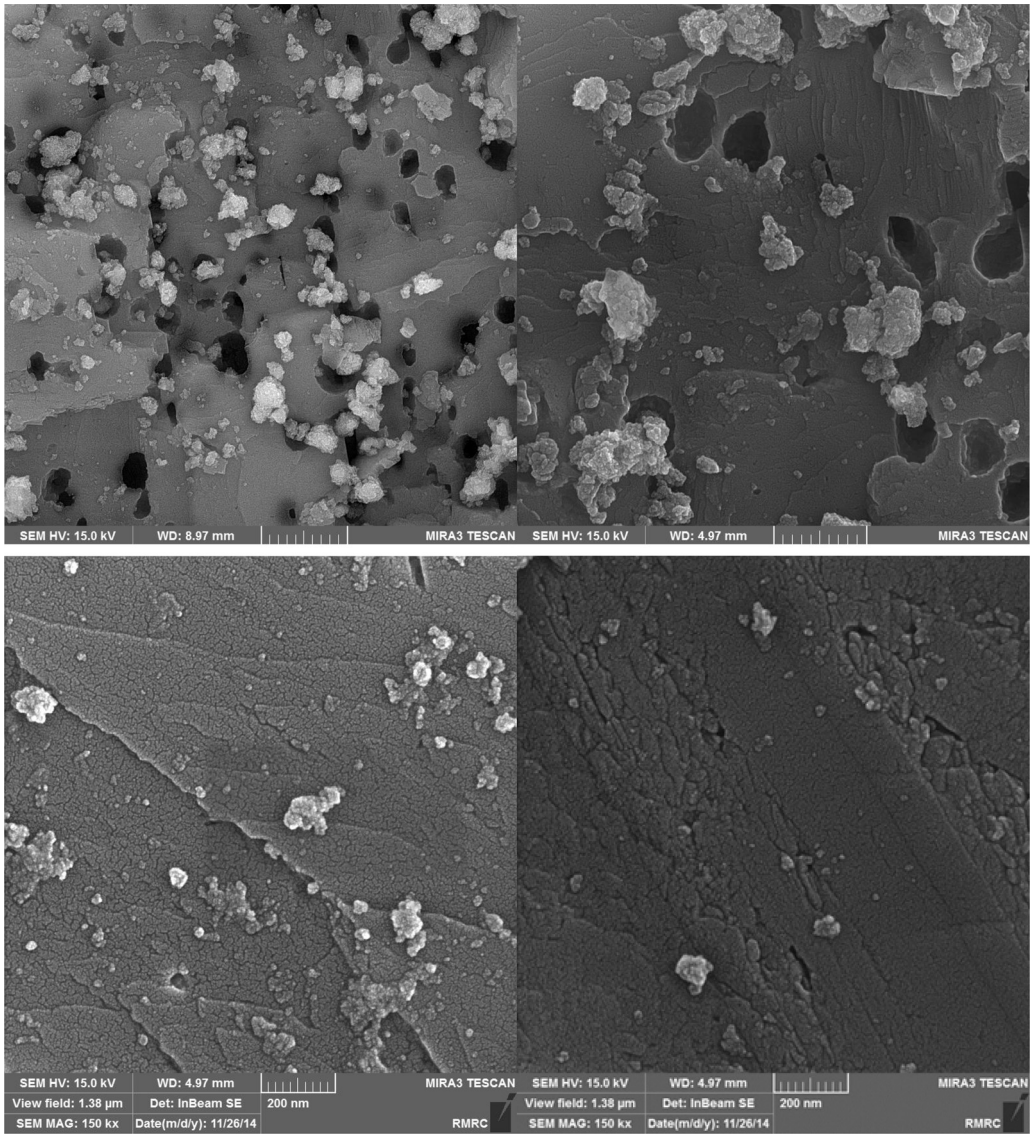

Fig. 13. FESEM images of Cu/eggshell nanocomposite.

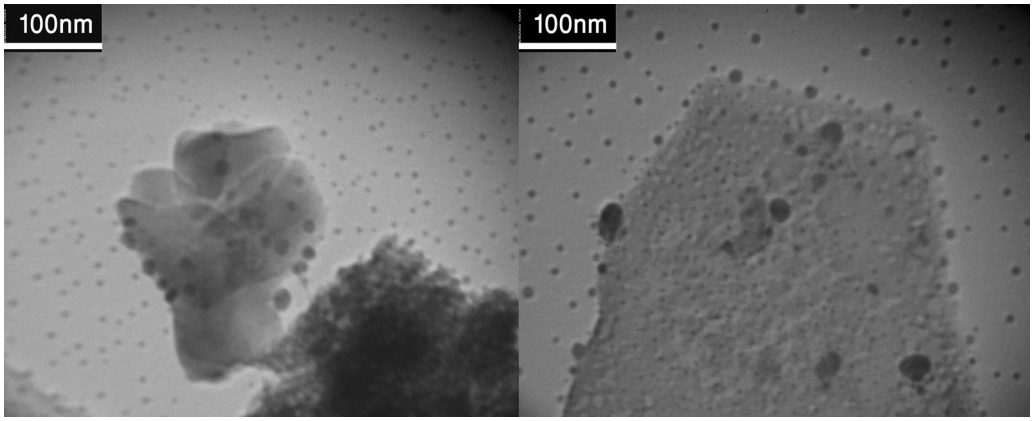

Fig. 14. TEM images of Cu/eggshell nanocomposite.

3.7. Preparation of Cu/Fe_3O_4/eggshell nanocomposite

In this study, for the first time, we demonstrated that eggshell can be utilized for *in situ* copper and iron nanoparticles preparation by reduction of copper and iron ions absorbed on the surface eggshell with a suitable reducing agent such as aqueous extract of the leaves of *Orchis mascula* L. and can be used as catalyst.

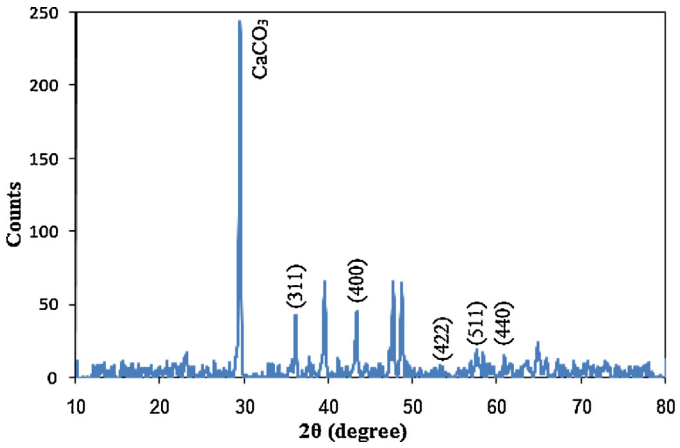

Fig. 15. XRD powder pattern of Fe_3O_4/eggshell nanocomposite.

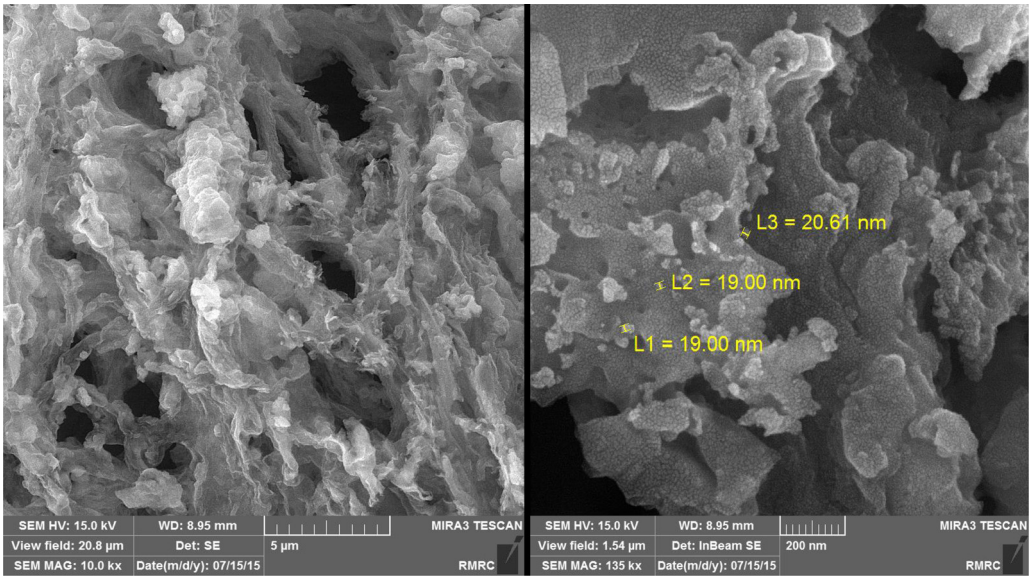

Fig. 16. FESEM images of Fe_3O_4/eggshell nanocomposite.

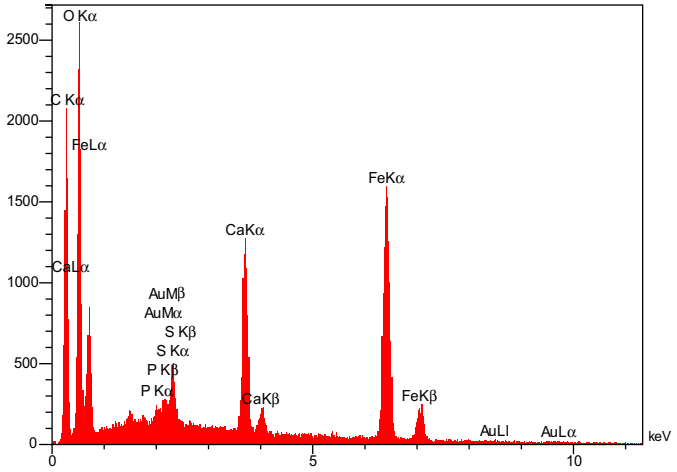

Fig. 17. EDS spectrum of Fe_3O_4/eggshell nanocomposite.

The structure and morphology of the product was examined by XRD and FESEM.

Fig. 19 shows a typical XRD pattern of Cu/Fe_3O_4/eggshell magnetic nanocomposite. The strong and sharp peak at $2\theta = 29.5^\circ$ is the characteristic peak of $CaCO_3$ [49]. The diffraction peaks at 2θ

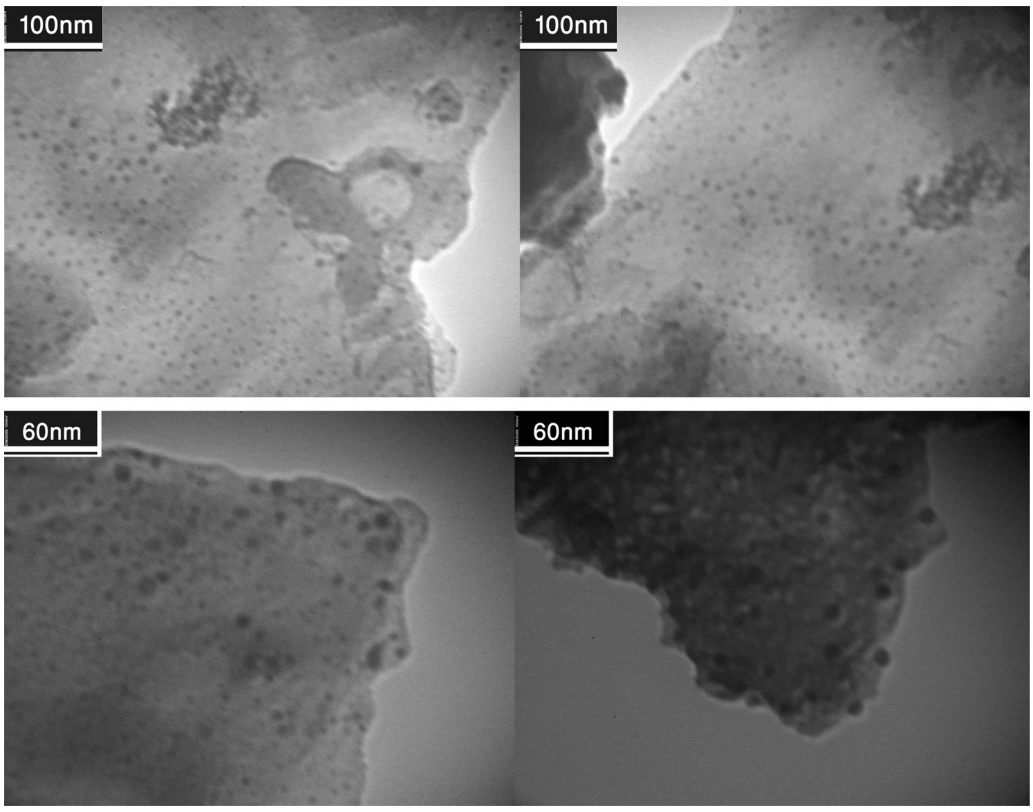

Fig. 18. TEM images of Fe_3O_4/eggshell nanocomposite.

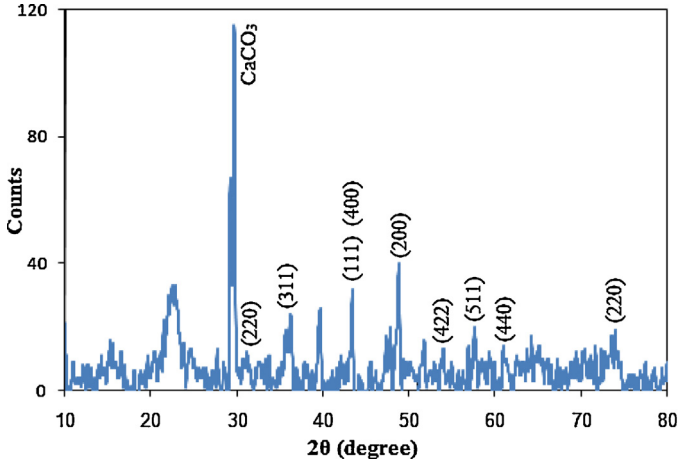

Fig. 19. XRD powder pattern of Cu/Fe_3O_4/eggshell nanocomposite.

value of 43.4°, 48.1° and 74.1° corresponding, respectively, to Cu (111), (200) and (220) crystalline plane appears, in accordance with Cu immobilization. XRD analysis shows major diffraction peaks at 30.09°, 35.6°, 43.4°, 54.6°, 57.6° and 62.0° (2θ), which can be indexed to (220), (311), (400), (422), (511) and (440) planes of the cubic Fe_3O_4 (JCPDS 19-0629).

Further, the presence of copper and iron was approved with EDS analysis (Fig. 20). The amount of Fe and Cu incorporated into the Cu/Fe_3O_4/eggshell nanocomposite found to be 46.32 wt% and 9.80 wt%, respectively which determined by EDS.

Fig. 21 shows typical FESEM images of the as-produced Cu/Fe_3O_4/eggshell nanocomposite. The eggshell porous is almost "coated" with Cu and Fe_3O_4 NPs. According to the literature and Fig. 8, the eggshell powder particles consist of highly porous structure [22–37], which increased the contact area and was responsible for Cu and Fe_3O_4 NPs loading onto eggshell powder particles. It can easily be seen in Figs. 8 and 21 that the presence of Cu and Fe_3O_4 NPs has caused changes in the roughness of the surface. The Cu and Fe_3O_4 particles with the average size about 17 nm uniformly distribute on the surface of the eggshell.

The elemental mapping images demonstrate that copper and iron nanoparticles are dispersed on the eggshell surface as evoked by XRD data (Fig. 22). Combined with the results of XRD and SEM for Cu/Fe_3O_4/eggshell nanocomposite we can confirm that Cu and Fe_3O_4 nanocrystallites were exactly fabricated on the eggshell surface.

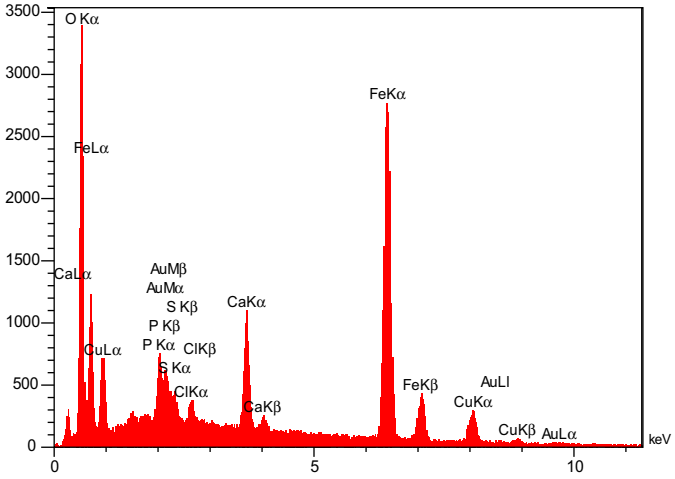

Fig. 20. EDS spectrum of Cu/Fe_3O_4/eggshell nanocomposite.

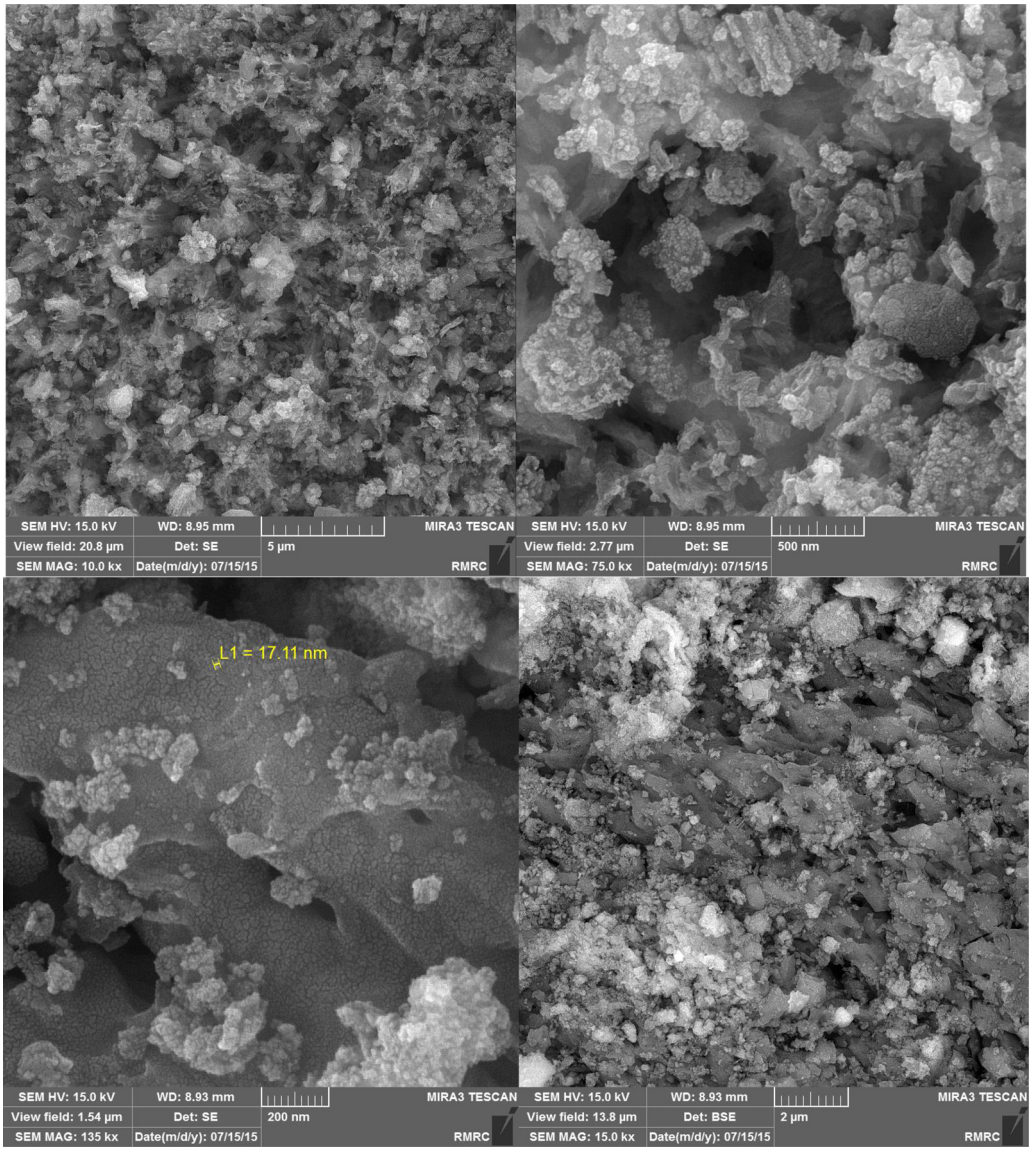

Fig. 21. FESEM images of Cu/Fe_3O_4/eggshell nanocomposite.

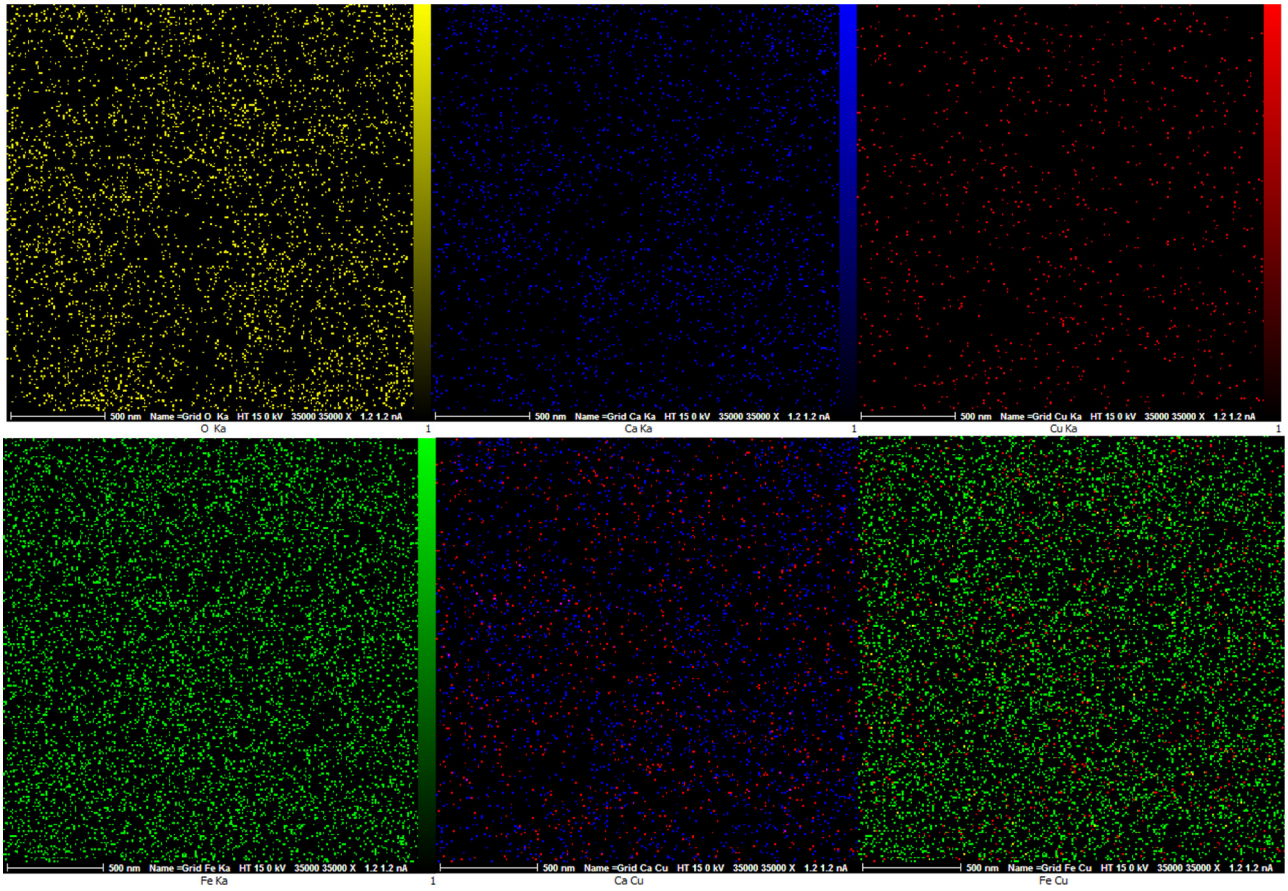

Fig. 22. Elemental mappings for (Yellow) O, (Blue) Ca, (Green) Fe and (Red) Cu. (For interpretation of the references to colour in this figure legend, the reader is referred to the web version of this article.)

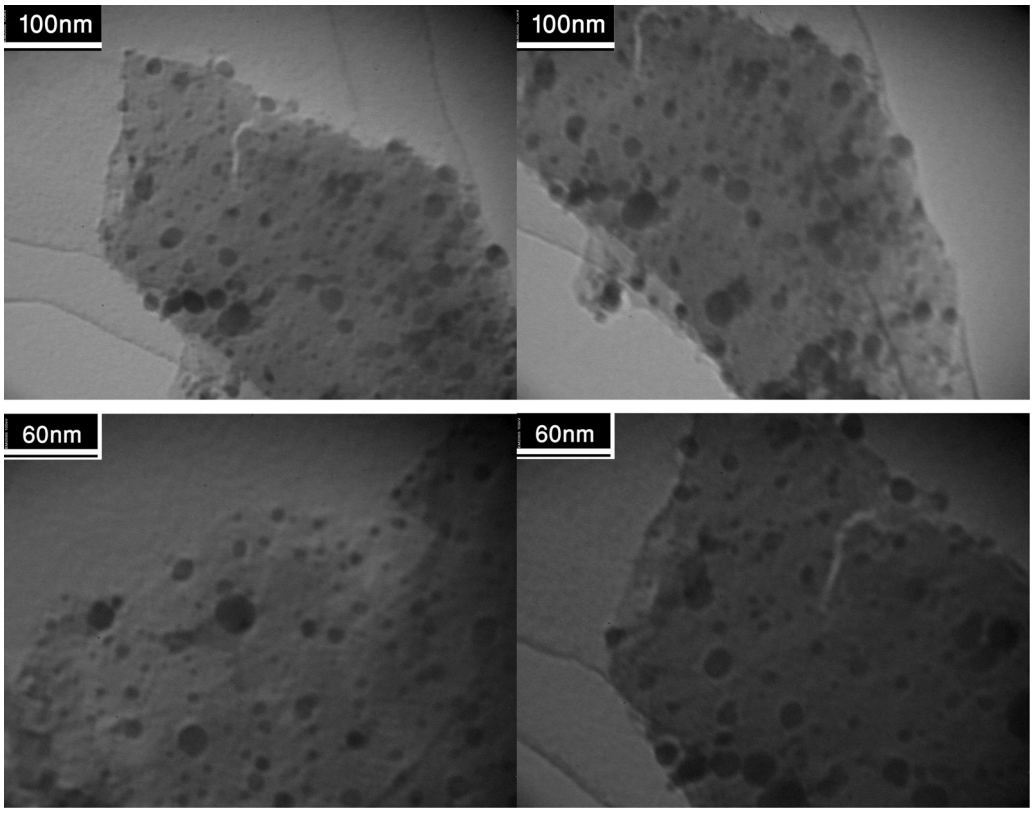

Fig. 23. TEM images of Cu/Fe_3O_4/eggshell nanocomposite.

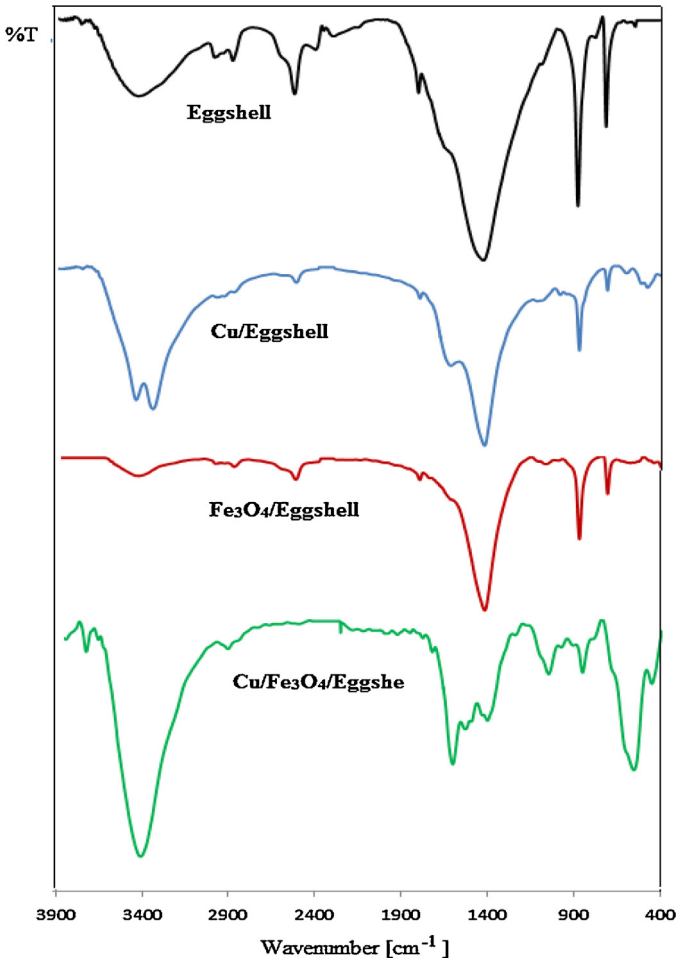

Fig. 24. FT-IR spectra of eggshell, Cu/eggshell, Fe_3O_4/eggshell and Cu/Fe_3O_4/eggshell nanocomposites.

Fig. 23 shows TEM images of Cu/Fe_3O_4/eggshell nanocomposite. TEM images indicated that the most of the prepared nanoparticles are spherical shaped and have sized 5–15 nm.

To confirm the functional groups on the adsorption media, the FT-IR spectra of the samples were collected in the 400–3900 cm^{-1} range (Fig. 24). The FT-IR studies of eggshell, Cu/eggshell, Fe_3O_4/eggshell and Cu/Fe_3O_4/eggshell nanocomposites confirm that there was no change in functional groups after the immobilization of Fe_3O_4 or Cu NPs on eggshell. In addition to existence of Fe_3O_4 in the samples as indicated by the XRD patterns, the peaks at 1075 and 3438 cm^{-1} correspond to the Fe-OH and O—H stretching modes of FeOH or adsorbed water. Furthermore, the peak around 1797 cm^{-1} indicates the carbonyl group stretching [51].

We furthermore analyzed the magnetic behavior of the Cu/Fe_3O_4/eggshell nanocomposite using a magnetometer at room temperature, with the field sweeping from −10000 to +10000 Oe. As shown in Fig. 25, the value of magnetic saturation for the Cu/Fe_3O_4/eggshell nanocomposite is 6.37 emu g^{-1}, indicating its magnetic nature. Thus, the catalyst could simply be separated by fixing a magnet near to the reaction vessel.

The thermal stabilities of the Cu/eggshell, Fe_3O_4/eggshell and Cu/Fe_3O_4/eggshell nanocomposites were also analyzed by TGA (thermogravimetric analysis) and DTA (differential thermal analysis) experiments in flowing air (120 mL min^{-1}) at a heating rate of 2 °C min^{-1} on an autonomic TG/DTA. As shown in Fig. S1A, two weight loss stages were observed in flowing air for the Cu/eggshell nanocomposite. About 14.0 wt% weight loss was observed in the first stage at 170–240 °C corresponding to desorption of surface

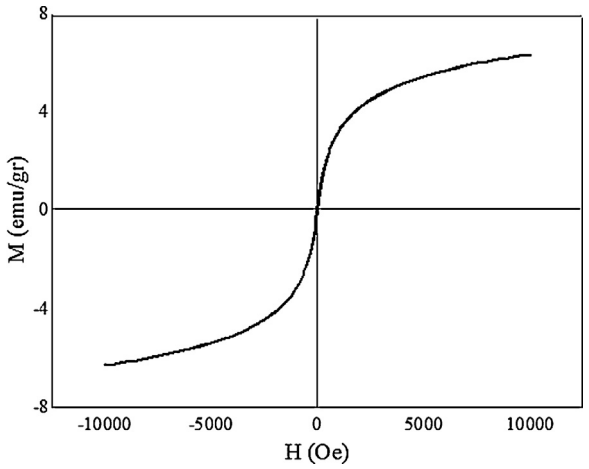

Fig. 25. VSM curve of the Cu/Fe_3O_4/eggshell nanocomposite.

water or decomposition of the organic content (leaf extract) present in the sample. In the second stage at >660 °C, a weight loss is observed which can be attributed to the decomposition of $CaCO_3$ to CaO and CO_2 [49]. We also analyzed thermal stabilities of the Fe_3O_4/eggshell and Cu/Fe_3O_4/eggshell nanocomposites after calcination at 400 °C. The weight loss of the Fe_3O_4/eggshell and Cu/Fe_3O_4/eggshell nanocomposites at >660 °C attributed to the decomposition of $CaCO_3$ to CaO and CO_2 (Fig. S1 B and S1C) [49].

The specific surface areas of Cu/eggshell and Cu/Fe_3O_4/eggshell nanocomposites were determined by BET (Brunauer–Emmett–Teller). The N_2 adsorption-desorption isotherm and Barrett–oyner–Halenda (BJH) pore size distribution plot of Cu/eggshell and Cu/Fe_3O_4/eggshell nanocomposites showed in Fig. S2 and S3 . Recent reports show that surface area, average pore diameter and pore volume of eggshell was 0.84 m^2/g, 0.0049 cm^3/g and 32.15 Å, respectively which indicated that natural eggshell processed low porosity [52,53]. The results indicate that the measured BET specific surface area of eggshell was increased after immobilization of copper and Fe_3O_4 nanoparticles. Based on isotherm curve, the measured BET surface area of Cu/eggshell and Cu/Fe_3O_4/eggshell nanocomposites were 22.77 m^2/g and 15.95 m^2/g, respectively. Moreover, the Barrett–Joyner–Halenda (BJH) analysis showed that the average pore diameter of Cu/eggshell nanocomposite is 12.0 nm and the pore volume is 6.84×10^{-2} cm^3/g, whereas the average pore diameter and pore volume of Cu/Fe_3O_4/eggshell nanocomposite is 13.4 nm and 5.34×10^{-2} cm^3/g, respectively. It is clear that number of pores on the surface of eggshell fairly increased after immobilization of copper and Fe_3O_4 nanoparticles.

3.8. Evaluation of the catalytic activity of Cu/eggshell, Fe_3O_4/eggshell and Cu/Fe_3O_4/eggshell nanocomposites through the reduction of variety of dyes

In situ synthesis of Cu NPs on the surface of eggshell yields uniform composites with strong catalytic activities. After confirming the exact characteristics of the catalyst, the catalytic activity of the Cu/eggshell, Fe_3O_4/eggshell and Cu/Fe_3O_4/eggshell nanocomposites were examined for reduction of 4-NP, MO, CR, MB and RhB in water at room temperature. The progress of the reaction was monitored by recording the absorption spectra as a function of time.

Initially, the reaction conditions were optimized for the reduction of 4-NP to 4-AP in the presence of different amounts of catalyst (Table 1). The amount of $NaBH_4$, as one of the factors influencing the reduction of 4-NP into 4-AP, was also investigated. As expected, no target product could be detected in the absence of catalyst. It can be

Table 1
Reduction of 4-NP catalyzed by different catalysts.

[4-NP] (mM)	[$NaBH_4$] (mM)	Catalyst (mg)	Time (min)
2.5	250	–	20:00
2.5	250	Eggshell (5.0)	20:00[a]
2.5	250	Cu NPs (5.0)	9:00
2.5	**250**	**Cu/eggshell (5.0)**	**1:40**
2.5	187.5	Cu/eggshell (5.0)	3:00
2.5	250	Cu/eggshell (10.0)	1:40
2.5	125	Cu/eggshell (5.0)	7:45
2.5	125	Cu/eggshell (10.0)	7:45
2.5	250	Fe_3O_4/eggshell (5.0)	5:35
2.5	250	Fe_3O_4/eggshell (7.0)	5:00
2.5	250	Cu/Fe_3O_4/eggshell (5.0)	4:46
2.5	250	Cu/Fe_3O_4/eggshell (7.0)	4:10

[a] Not completed.

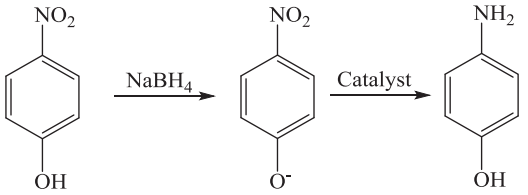

Fig. 26. The reduction of 4-NP in the presence of $NaBH_4$ and catalyst.

seen that the rate of reduction of 4-NP is increased on increasing the molar ratio of $NaBH_4$ to 4-NP. Nevertheless, the best results were achieved in the presence of 5.0 mg of Cu/eggshell and 100 equivalents of $NaBH_4$ (250 mM). The reduction reaction in the presence of eggshell as catalyst and in the absence of Cu NPs, was also performed, resulting in very low conversion. Compared with the Cu NPs prepared by aqueous extract of the leaves of *Orchis mascula* L., the Cu/eggshell nanocomposite showed apparently higher catalytic activity, which could be attributed to the effect of increased surface area, smaller size and the well dispersity of the Cu NPs fabricated on the eggshell. In a word, the NPs in eggshell exhibit good catalytic activity due to the highly porous structure of eggshell powder particles that provides a high accessibility to the NPs. On the other hand, the eggshell had good adsorption ability to the water-soluble 4-NP, which could accelerate the process of catalytic reduction. It suggested that the eggshell may play an active part in the catalysis, yielding a synergistic effect. The catalytic mechanism for the conversion of 4-NP into 4-AP relies on the electrons transfer from the BH_4^- donor to the acceptor 4-NP through adsorption of the reactant molecules on to the eggshell surface. The Cu NPs can serve as catalyst to transfer electrons from BH_4^- to the 4-NP, which are both absorbed on the catalysts via π-π stacking interactions, leading to the production of amino derivatives. In the present work, when the Cu/eggshell was added to a mixed solution of 4-nitrophenol (oxidant) and $NaBH_4$ (reductant), 4-nitrophenolate ions (Fig. 26) and BH_4^- were first adsorbed on the surface of the catalyst via physical adsorption. In contrast, without a highly adsorbent eggshell support, 4-NP must collide with Cu NPs by chance, and remains in contact for the catalysis to proceed. After electron transfer (ET) to the Cu NPs, the hydrogen atom forms from the hydride, and then attacks 4-nitrophenolate ions to reduce it. This ET-induced hydrogenation of 4-NP occurred spontaneously at the surface of the metal catalyst. Finally, the generated 4-AP was desorbed from the surface of the catalyst.

In addition, the catalytic activities of the Fe_3O_4/eggshell and Cu/Fe_3O_4/eggshell nanocomposites were also investigated. As shown, the time of reaction in the presence of Cu/eggshell is better than Cu NPs, Fe_3O_4/eggshell and Cu/Fe_3O_4/eggshell nanocomposites. According to the EDS results (Figs. 11 and 20), the amount of Cu NPs in Cu/eggshell is higher than Cu/Fe_3O_4/eggshell nanocomposite. This result clearly demonstrates that the Cu NPs are necessary for this reduction process and the catalytic reduction occurs at the surface of catalyst. For this reason, the Cu/eggshell prepared with the leaf extract of *Orchis mascula* L. as a stabilizing and reducing agent had a more excellent catalytic performance than Cu NPs and Cu/Fe_3O_4/eggshell nanocomposites. Therefore, the Cu/eggshell provides great advantages for the use in the reduction of 4-NP due to the high surface area and good catalytic activity. However, the magnetism of the Fe_3O_4/eggshell and Cu/Fe_3O_4/eggshell nanocomposites made them easy to recycle. The Fe_3O_4/eggshell and Cu/Fe_3O_4/eggshell nanocomposites powder could be removed conveniently from water with the help of an external magnet.

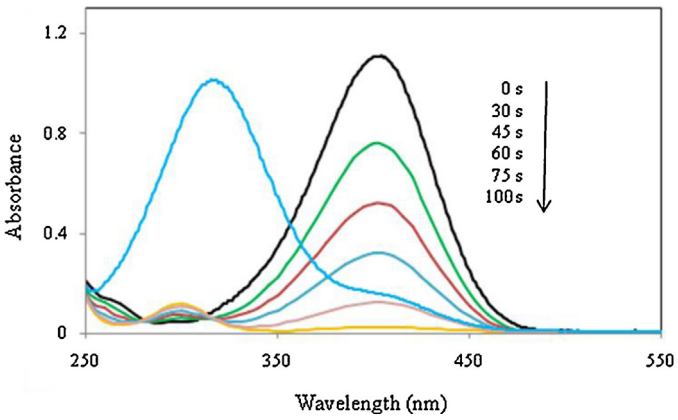

Fig. 27. UV–vis spectra for catalytic reduction of 4-NP to 4-AP at several interval, conditions: [4-NP] = 2.5×10^{-3} M, [$NaBH_4$] = 0.25 M, Cu/eggshell = 5.0 mg.

As shown in Fig. 27, 4-NP in aqueous medium has a maximum absorption at 317 nm. The light yellow color of the solution changed to intense yellow when 25 mL of the newly prepared $NaBH_4$ (0.25 M) was added into 4-NP and showed an absorption peak at about 400 nm which did not change as time passed. This was due to the formation of 4-nitrophenolate ions in alkaline condition. The peak at 400 nm remains unchanged even for a couple of days in the absence of catalyst. After the catalyst was added into the solution containing 4-NP and $NaBH_4$, the intensity of the strong absorption peak at 400 nm gradually decreased and a new peak appeared at about 300 nm which corresponded to the formation of 4-AP. After about 100 s in case of Cu/eggshell, the whole peak at 400 nm almost disappeared and the color became transparent, which indicated that 4-NP was almost turned to 4-AP.

In our reaction system the concentration of $NaBH_4$ is significantly higher than that of 4-NP. Hence, the rate of reduction is independent of the concentration of $NaBH_4$ and the reaction considered as pseudo-first order reaction with respect to p-NP alone [54–63]. The kinetic equation for the reduction could be written as follows:

$$dC_t/dt = dA_t/dt = kC_t or ln(C_t/C_0) = ln(A_t/A_0) = -kt$$

where, C_t is the concentration of 4-NP in the reaction time t, C_0 is the initial concentration of 4-NP, A_t is the absorbance at any time t and A_0 is the absorbance at time t = 0 and k is the rate constant. The plots of $ln(A_t/A_0)$ versus time (t) for the catalytic reduction of 4-NP in the presence of Cu/eggshell, Fe_3O_4/eggshell and Cu/Fe_3O_4/eggshell nanocomposites and $NaBH_4$ are shown in Fig. 28. As shown in Fig. 28, the linear correlation between $ln(A_t/A_0)$ and reaction time demonstrates that the reduction of 4-NP by Cu/eggshell, Fe_3O_4/eggshell or Cu/Fe_3O_4/eggshell nanocomposites is of pseudo first-order. The kinetic reaction rate constants (k) values are 1.74, 0.84 and 0.72 min^{-1} for Cu/eggshell, Fe_3O_4/eggshell and Cu/Fe_3O_4/eggshell nanocomposites, respectively.

Table 2
Comparison of reduction time and rate constant values for the reduction of 4-NP to 4-AP by $NaBH_4$ in the presence of various catalysts.

Catalyst	Concentration of 4-NP (mM) [mmol]	Concentration of $NaBH_4$ (mM) [mmol]	Time (min)	k (min^{-1})	Ref.
$NiFe_2O_4$ NPs	36 [0.72]	1798 [36]	16	0.12	[54]
Ni NPs	0.1 [3×10^{-4}]	200 [0.06]	16	0.16	[55]
Ni/graphene nanocomposite	0.1 [2×10^{-3}]	132 [0.26]	4	0.7	[56]
Cu-Fe_3O_4@graphene composite	1 [0.01]	92.5 [1.85]	5	0.7	[57]
Pd-graphene nanohybrid	0.1 [2.9×10^{-4}]	10 [1×10^{-3}]	12	0.14	[58]
Cu_3Ni_2 bimetallic nanocrystals	0.1 [2×10^{-3}]	20 [0.1]	6	0.58	[59]
$NiCo_2$ alloy microstructure	0.1 [1×10^{-3}]	60 [0.6]	30	0.07	[60]
$FeNi_2$ alloy nanostructure	0.1 [1×10^{-4}]	60 [0.06]	60	0.06	[61]
Au NPs/ionic liquid-graphene	0.025 [3.7×10^{-5}]	2.5 [3.8×10^{-3}]	7	0.40	[62]
Au-Pd bimetallic NPs/graphene	0.1 [1×10^{-5}]	10 [0.01]	3.5	0.87	[63]
Cu/eggshell nanocomposite	2.5 [0.05]	250 [6.25]	100 s	1.74	This work

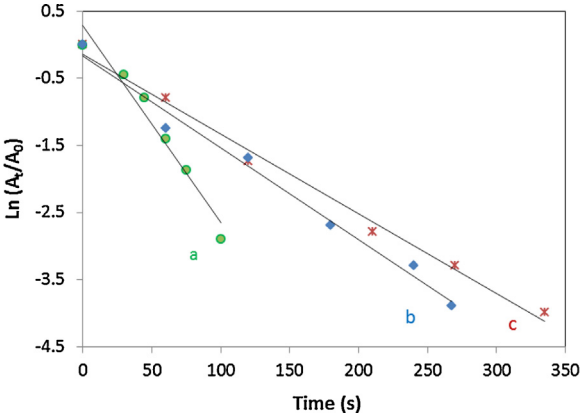

Fig. 28. Plots of $\ln(A_t/A_0)$ vs. irradiation time for reduction reaction of 4-NP (2.5×10^{-3} M). Conditions: (a) [$NaBH_4$] = 250 mM; Cu/eggshell = 5.0 mg; (b) [$NaBH_4$] = 250 mM; Fe_3O_4/eggshell = 7.0 mg; b) [$NaBH_4$] = 250 mM; Cu/Fe_3O_4/eggshell = 7.0 mg.

The catalytic performance of the catalyst Cu/eggshell nanocomposite and comparison with various reference catalysts were firstly assessed in the reduction of 4-NP using $NaBH_4$ as reductant at room temperature in aqueous medium, the results are listed in Table 2. It can be seen that the reaction did not proceed at all in the absence of catalyst. Further, as compared in Table 2, the rate constant for the Cu/eggshell nanocomposite is also larger than those reported in recent catalytic systems.

In the next step, we then turned our attention to applying Cu/eggshell for the reduction of CR, MO, MB and RhB in the presence of excess $NaBH_4$ (Scheme 4). The reaction progress was monitored by UV–vis spectroscopy.

In the exploratory experiments, the effect of various catalysts was examined. The results (Table 3) show that the reaction in the presence of Cu/eggshell gives the highest conversion. Lower catalytic activities are observed using other catalysts.

The catalytic reductions of dyes were monitored by UV–vis spectrometer, as illustrated in Fig. 29, CR, MO, MB and RhB in water solution exhibits a peak at 493, 465, 663 and 554 nm, respectively, after the addition of aqueous $NaBH_4$ and catalyst the whole absorbance peak almost disappeared within 10–120 s, depending upon the dye.

In order to show the applicability and efficiency of our catalytic system, results are compared with some of the recently reported methods for the reduction of variety of dyes by $NaBH_4$ (Table 4). Our method is the shortest time for the reduction of organic dyes reported in the literatures, so far.

Compared with the other literature works on the reduction of organic dyes, the notable features of our method are:

Table 3
Effect of various catalysts in the reduction of MB, RhB, CR and MO with $NaBH_4$.

Dye (M)	[$NaBH_4$] (M)	Catalyst (mg)	Time (min)
CR	5.3×10^{-3}	Eggshell (5.0)	30:00[a]
(1.44×10^{-5})	5.3×10^{-3}	Cu/eggshell (3.0)	30:00[b]
	5.3×10^{-3}	Cu/eggshell (5.0)	1:26
	5.3×10^{-3}	**Cu/eggshell (7.0)**	**1:05**
	5.3×10^{-3}	Fe_3O_4/eggshell (5.0)	20:00[a]
	5.3×10^{-3}	Fe_3O_4/eggshell (7.0)	1:56
	5.3×10^{-3}	Cu/Fe_3O_4/eggshell (5.0)	25:00[a]
	5.3×10^{-3}	Cu/Fe_3O_4/eggshell (7.0)	2:10
MB	5.3×10^{-3}	Eggshell (5.0)	90:00[c]
(3.1×10^{-5})	5.3×10^{-3}	Cu NPs (3.0)	1:00
	5.3×10^{-3}	Cu/eggshell (1.0)	6:18
	5.3×10^{-3}	**Cu/eggshell (3.0)**	**10 s**
	5.3×10^{-3}	Cu/eggshell (5.0)	10 s
	5.3×10^{-3}	Fe_3O_4/eggshell (3.0)	90:00[c]
	5.3×10^{-3}	Fe_3O_4/eggshell (5.0)	90:00[c]
	5.3×10^{-3}	Fe_3O_4/eggshell (5.0)	90:00[c]
	5.3×10^{-3}	Cu/Fe_3O_4/eggshell (3.0)	30:00[a]
	5.3×10^{-3}	Cu/Fe_3O_4/eggshell (10.0)	34 s
RhB	5.3×10^{-3}	Eggshell (5.0)	60:00[c]
(2.09×10^{-5})	5.3×10^{-3}	Cu/eggshell (5.0)	30:00[a]
	5.3×10^{-3}	Cu/eggshell (7.0)	30:00[d]
	5.3×10^{-3}	**Cu/eggshell (10.0)**	**1:30**
	5.3×10^{-3}	Cu/eggshell (20.0)	1:30
	5.3×10^{-3}	Cu/Fe_3O_4/eggshell (10.0)	25:00[d]
MO	5.3×10^{-3}	Eggshell (7.0)	45:00
(3.0×10^{-5})	5.3×10^{-3}	Cu NPs (7.0)	18:33
	5.3×10^{-3}	Cu/eggshell (5.0)	2:09
	5.3×10^{-3}	**Cu/eggshell (7.0)**	**2:00**
	5.3×10^{-3}	Fe_3O_4/eggshell (7.0)	13:00
	5.3×10^{-3}	Cu/Fe_3O_4/eggshell (5.0)	17:00
	5.3×10^{-3}	Cu/Fe_3O_4/eggshell (7.0)	12:14

[a] Not completed.
[b] The conversion is 90%.
[c] No reaction.
[d] The conversion is 80%.

- The use of waste chicken eggshell as a natural and inexpensive valuable resource and environmentally benign support;
- The use of plant extract as an economic and effective alternative represents an interesting, fast and clean synthetic route for the synthesis of Cu/eggshell, Fe_3O_4/eggshell and Cu/Fe_3O_4/eggshell nanocomposites without use of toxic, hazardous and dangerous materials or surfactant, capping agent and/or template;
- The synthesized catalysts by this method are quite stable and could be kept for several months;
- The reaction system is simple;
- Elimination of homogeneous catalysts;
- The time of the reaction is short; and
- The catalysts could be easily recovered and reused;

These advantages make the present method to be considered as a convenient alternative method for the reduction of organic dyes.

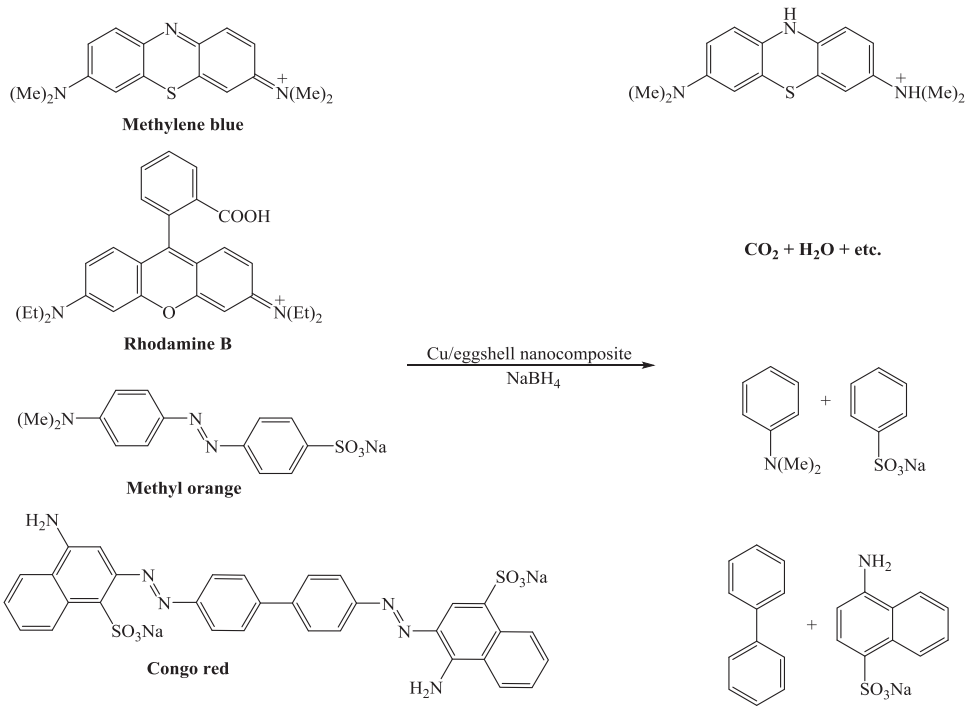

Scheme 4. Mechanism of the catalytic reduction and degradation of dyes with Cu/eggshell nanaocomposite.

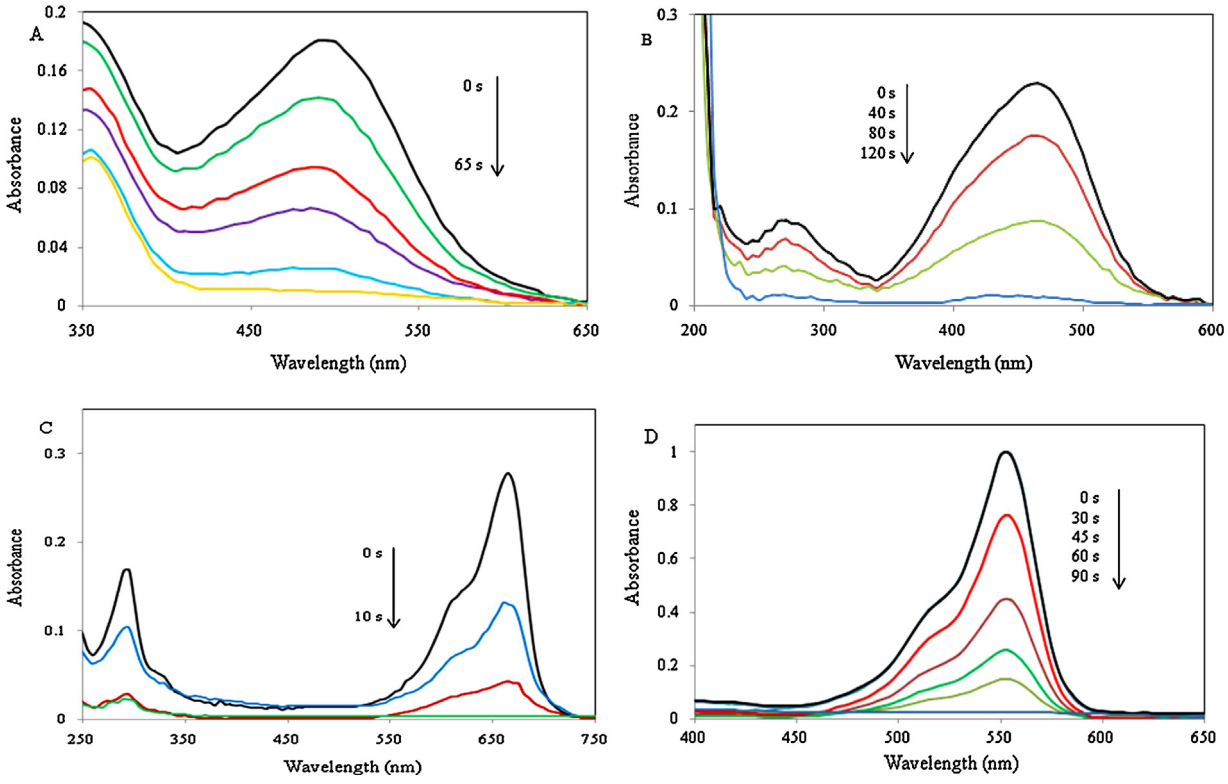

Fig. 29. UV–vis spectra of the catalytic reduction of CR (A), MO (B), MB (C) and RhB (D) in aqueous solution recorded at various time intervals using Cu/eggshell nanocomposite.

3.9. Catalyst recyclability

For the application as a practical catalyst, the catalytic stability and the reuse of the catalyst are very important. The recovery and reusability of the Cu/eggshell nanocomposite was investigated in the reduction of 4-NP to 4-AP under the optimized conditions. After completion of the reaction, the catalyst was separated from the reaction mixture by centrifugation, washed three times with doubly distilled water, dried in an oven at 100 °C for 2 h and the recycled catalyst was saved for the next reaction. It is found that Cu/eggshell

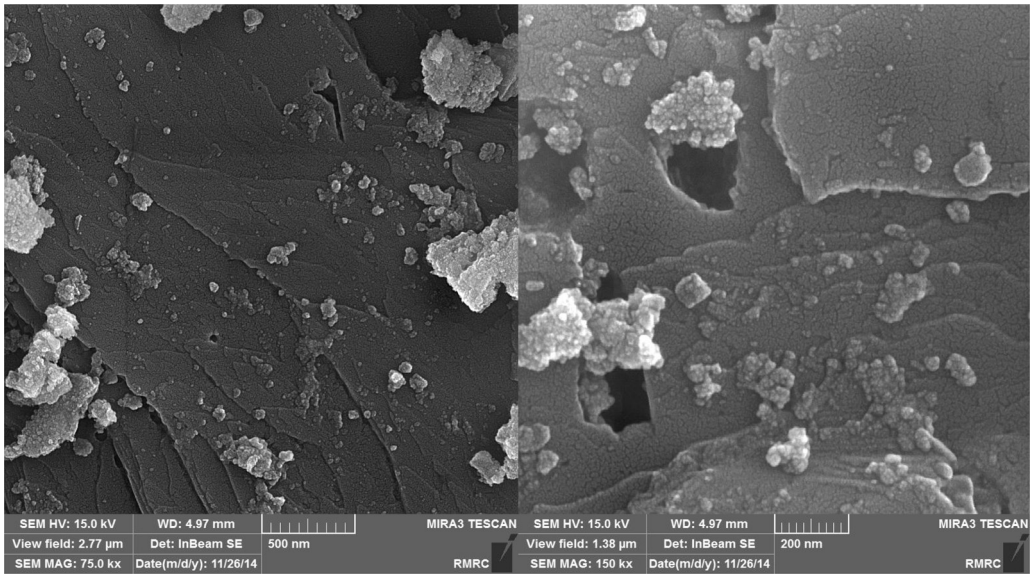

Fig. 30. FESEM image of recovered Cu/eggshell nanocomposite.

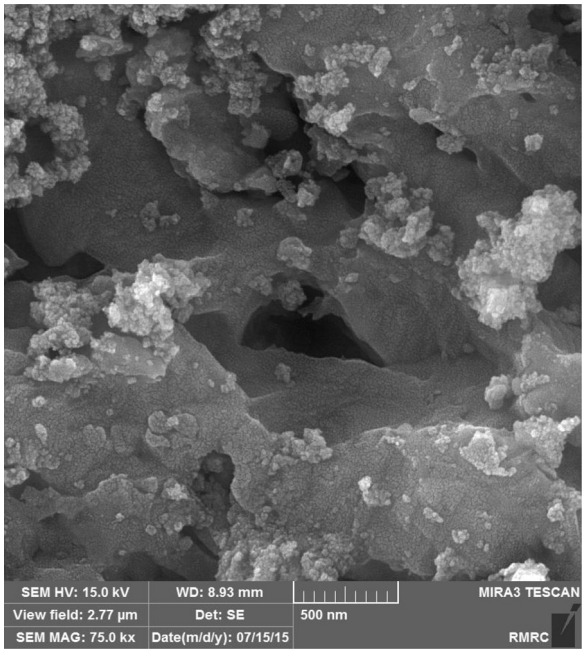

Fig. 31. FESEM image of recovered Cu/Fe_3O_4/eggshell nanocomposite.

nanocomposite does not lose its catalytic activity during at least seven catalytic cycles in the reduction of 4-NP with $NaBH_4$. In addition, the catalytic efficiency of the catalyst remained almost constant up to seven cycle of operation and the time required for 100% reduction of RhB, MO, CR and MB was found to be almost same up to the 7th cycle. The reusability of the Fe_3O_4/eggshell and Cu/Fe_3O_4/eggshell were studied for the reduction of dyes. After completion of the reduction reaction, the catalyst was separated from the reaction mixture with an external magnet, washed with doubly distilled water, dried in a hot air oven at 100 °C for 2 h and reused for a consecutive run under the same reaction conditions. The recycled catalyst could be reused seven times with no loss of activity. The FESEM image of the recovered Cu/eggshell and Cu/Fe_3O_4/eggshell nanocomposites revealed that the nanoparticles were identical in shape and size even after the 7th run (Fig. 30 and 31).

4. Conclusions

In conclusion, we have described a facile and green route to prepare Cu/eggshell, Fe_3O_4/eggshell and Cu/Fe_3O_4/eggshell nanocomposites using aqueous extract of the leaves of *Orchis mascula* L. as a stabilizing and reducing agent. The nanocomposites were characterized by FESEM, EDS, TEM, XRD, BET, VSM, DTA-TGA and FT-IR techniques. The formed Cu and Fe_3O_4 particles uniformly distributed on the eggshell surface. The research opens a new insight to design low-cost, highly active and stable catalysts for reduction of 4-NP, MO, CR, MB and RhB in water at room temperature. The facile synthesis, excellent properties, alterable supports and low costs allow these nanocomposites to be used in reduc-

Table 4
Comparison of results for the reduction of variety of dyes by $NaBH_4$ in the presence of various catalysts.

Substrate	Catalyst	Time	Ref.
4-NP	GA-Pt NPs	8 h	[64]
	Pd-FG	12 min	[65]
	Au@PZS@CNTs	16 min	[66]
	Ni-PVAm/SBA-15	85 min	[67]
	TiO_2-$G_{1\%}$	60 min	[68]
	Fe_3O_4@C@Pt	60 min	[69]
	Cu NPs	2 h	[70]
	HMMS-NH_2-Pd	60 min	[71]
	p(AMPS)-Ni composite	5.5 h	[72]
	PdCu/graphene	1.5 h	[73]
	KCC-1/Au	12 min	[74]
	Ag/KCC-1	510 s	[75]
	Resin-Au NPs	20 min	[76]
	NAP-Mg-Au(0)	7 min	[77]
	Polymer-anchored Pd(II) complex	5.5 h	[78]
	Au-GO	30 min	[79]
	Au/graphene hydrogel	720 s	[80]
	Pd-FG	12 min	[81]
	p(AMPS)-Co composite	28 min	[82]
	Cu NPs/perlite	2.5 min	[83]
	Cu/eggshell nanocomposite	100 s	This work
MB	Porous Cu microspheres	8 min	[84]
	SiNWAs-Cu	10 min	[85]
	Au/Fe_3O_4@C	10 min	[86]
	Ag NPs on silica spheres	7.5 min	[87]
	Au_{core}-$PANI_{shell}$	5 min	[88]
	copper nanocrystals	200 s	[89]
	Cu/eggshell nanocomposite	10 s	This work
RhB	SiNWAs-Cu	14 min	[85]
	Fe_3O_4@PANI@Au	18 min	[90]
	Au-PANI nanocomposite	15 min	[91]
	Fe_3O_4/Ag	15 min	[92]
	Ag/$HLaNb_2O_7$	47 min	[93]
	PS/Ag	10 min	[94]
	copper nanocrystals	300 s	[95]
	Cu/eggshell nanocomposite	90 s	This work
CR	copper nanocrystals	500 s	[89]
	Cu@SBA-15	7 min	[95]
	Cu/eggshell nanocomposite	65 s	This work
MO	Cu@SBA-15	5 min	[95]
	Cu/eggshell nanocomposite	2 min	This work

tion of variety of dyes and other fields. The nanocomposites could be readily recovered and reused for several cycles with no loss of activity. Moreover, the present synthesis procedure is a sort of green, simple, moderate, effective, environmental and economical strategy for the preparation of other composites with eggshell and other biomaterials as supports. The synthesis and characterization of nanocomposites utilizing bones, oysters and shells in the presence of plant extracts are currently in progress in our research group.

Supporting information available

DTA-TGA data measured for Cu/eggshell, Fe_3O_4/eggshell and Cu/Fe_3O_4/eggshell nanocomposites calcined at 400 °C and the N_2 adsorption-desorption isotherm and Barrett–Joyner–Halenda (BJH) pore size distribution plot of Cu/eggshell and Cu/Fe_3O_4/eggshell nanocomposites.

Acknowledgments

We gratefully acknowledge the Iranian Nano Council and the University of Qom for the support of this work.

Appendix A. Supplementary data

Supplementary data associated with this article can be found, in the online version, at http://dx.doi.org/10.1016/j.apcatb.2016.02.042.

References

[1] C.A. Martinez-Huitle, E. Brillas, Appl. Catal. B 87 (2009) 105–145.
[2] M. Nasrollahzadeh, S.M. Sajadi, A. Rostami-Vartooni, M. Alizadeh, M. Bagherzadeh, J. Colloid Interface Sci. 466 (2016) 360–368.
[3] B.Y. Su, Y.Z. Jia, S.Q. Zhang, X.M. Chen, M. Oyama, Chem. Lett. 43 (2014) 919–921.
[4] E. Seo, J. Kim, Y. Hong, Y.S. Kim, D. Lee, B.S. Kim, J. Phys. Chem. C 117 (2013) 11686–11693.
[5] S. Laurent, D. Forge, M. Port, A. Roch, C. Robic, L.V. Elst, R.N. Muller, Chem. Rev. 108 (2008) 2064–2110.
[6] Y. Isomura, T. Narushima, H. Kawasaki, T. Yonezawa, Y. Obora, Chem. Commun. 48 (2012) 3784–3786.
[7] C. Guang, T. Yong-jian, L. Wei, L. Jiang-shan, L. Jun, Y. Tian-zu, Met. Funct. Mater. 12 (3) (2005) 18–21.
[8] C. Qing-chun, Fine Chem. 22 (6) (2005) 417–419.
[9] G. Xin-ling, S. Zheng-tao, Appl. Chem. Ind. 34 (10) (2005) 615–617.
[10] W. Xiao-li, X. Bin-shi, Y. He-long, X. Yi, Chin Surf. Eng. 18 (5) (2005) 24–27.
[11] H. Feng, Z. Zheng-yi, X. Yao-fu, W. Wu-xiang, H. Ya-fang, W. Run, Acta Metall. Sin. 36 (6) (2000) 659–661.
[12] W. Qi-feng, Z. Qi-xiu, Non-ferrous Smelt. 6 (3) (2003) 10–13.
[13] H. Li-jun, H. Cai-xia, W. Yong-hong, J. Gansu Lianhe Univ. Nat. Sci. 19 (4) (2005) 49–51.
[14] T. Ling-hua, L. Feng-sheng, J. Nanjing Inst. Tech. Nat. Sci. Ed. 3 (1) (2005) 6–10.
[15] M. Nasrollahzadeh, N. J. Chem. 38 (2014) 5544–5550.
[16] M. Atarod, M. Nasrollahzadeh, S.M. Sajadi, J. Colloid Interface Sci. 465 (2016) 249–258.
[17] M. Nasrollahzadeh, S.M. Sajadi, J. Colloid Interf. Sci. 462 (2016) 243–251.
[18] M. Nasrollahzadeh, S.M. Sajadi, J. Colloid Interface Sci. 465 (2016) 121–127.
[19] M. Nasrollahzadeh, M. Maham, A. Rostami-Vartooni, M. Bagherzadeh, S.M. Sajadi, RSC Adv. 5 (2015) 64769–64780.
[20] M. Nasrollahzadeh, S.M. Sajadi, J. Colloid Interface Sci. 464 (2016) 147–152.
[21] A. Hatamifard, M. Nasrollahzadeh, J. Lipkowski, RSC Adv. 5 (2015) 91372–91381.
[22] W.J. Stadelman, Encyclopedia of Food Science and Technology, 2nd ed., John Wiley and Sons, New York, 2000, pp. 593–599.
[23] N.Y. Mezenner, A. Bensmaili, Chem. Eng. J. 147 (2009) 87–95.
[24] Z. Wei, C. Xu, B. Li, Biores. Technol. 100 (2009) 2883–2885.
[25] S. Yoo, J.S. Hsieh, P. Zou, J. Kokoszka, Biores. Technol. 100 (2009) 6416–6421.
[26] C. Balázsi, F. Wéber, Z. Köver, E. Horváth, C. Németh, J. Eur. Ceram. Soc. 27 (2007) 1601–1606.
[27] D. Yang, L.M. Qi, J.M. Ma, Adv. Mater. 14 (2002) 1543–1546.
[28] T.X. Fan, S.K. Chow, Z. Di, Prog. Mater. Sci. 54 (2009) 542–659.
[29] W. Zhang, D. Zhang, T.X. Fan, J.J. Gu, R. Ding, H. Wang, Q.X. Guo, H. Ogawa, Chem. Mater. 21 (2009) 33–40.
[30] V. Valtchev, F.F. Gao, L. Tosheva, N. J. Chem. 32 (2008) 1331–1337.
[31] W.T. Tsai, K.J. Hsien, H.C. Hsu, C.M. Lin, K.Y. Lin, C.H. Chiu, Bioresour. Technol. 99 (2008) 1623–1629.
[32] L. Dupoirieux, D. Pourquier, F. Souyris, J. Craniomaxillofacial Surg. 23 (1995) 187–194.
[33] D. Liao, W. Zheng, X. Li, Q. Yang, X. Yue, L. Guo, G. Zeng, J. Hazard. Mater. 177 (2010) 126–130.
[34] N. Viriya-empikul, P. Krasae, B. Puttasawat, B. Yoosuk, N. Chollacoop, K. Faungnawakij, Bioresour. Technol. 101 (2010) 3765–3767.
[35] Y.C. Sharma, B. Singh, J. Korstad, Energy Fuels 24 (2010) 3223–3231.
[36] A. Montilla, M.D. del Castillo, M.L. Sanz, A. Olano, Food Chem. 90 (2005) 883–890.
[37] Y. Gao, C. Xu, Catal. Today 190 (2012) 107–111.
[38] B. Pant, Afr. J. Plant Sci. 7 (10) (2013) 448–467.
[39] H.S.K. Agrawal, Int. J. Clin. Pract. 2 (2003) 29–31.
[40] M. Darukhshan Kalim, D. Bhattacharyya, A. Banerjee, S. Chattopadhyay, BMC Complement. Altern. Med. 10 (2010) 77.
[41] H. Jacquemyn, R. Brys, O. Honnay, M.J. Hutchings, J. Ecol. 97 (2009) 360–377.
[42] N. Aziz, M. Hassan Mehmood, H. Salman Siddiqi, S.-U. Rehman Mandukhail, F. Sadiq, W. Maan, A. Hassan Gilani, Hypertens. Res. 32 (2009) 997–1003.
[43] L. Dormont, R. Delle-Vedove, J.-M. Bessière, B. Schatz, Phytochemistry 100 (2014) 51–59.
[44] S.V. Bhat, B.A. Nagasampagi, M. Sivakumar, Chemistry of Natural Products, Narosa Publishing House, New Delhi, 2005, pp. 585–683.
[45] M. Atarod, M. Nasrollahzadeh, S.M. Sajadi, J. Colloid Interface Sci. 462 (2016) 272–279.
[46] M. Nasrollahzadeh, S.M. Sajadi, J. Colloid Interface Sci. 462 (2016) 243–251.
[47] M. Nasrollahzadeh, M. Atarod, S.M. Sajadi, Appl. Surf. Sci. 364 (2016) 636–644.
[48] I.F.F. Benzie, J.J. Strain, Anal. Biochem. 239 (1996) 70–76.
[49] E. Mosaddegh, A. Hassankhani, Catal. Commun. 33 (2013) 70–75.
[50] A. Layek, G. Mishra, A. Sharma, M. Spasova, S. Dhar, A. Chowdhury, R. Bandyopadhyaya, J. Phys. Chem. C 116 (2012) 24757–24769.

[51] Q. Gao, F.H. Chen, J.L. Zhang, G.Y. Hong, J.Z. Ni, X. Wei, D.J. Wang, J. Magn, Magn. Mater. 321 (2009) 1052–1057.
[52] W.T. Tsai, J.M. Yang, C.W. Lai, Y.H. Cheng, C.C. Lin, C.W. Yeh, Bioresour. Technol. 97 (2006) 488–493.
[53] Y. Gao, C. Xu, Catal. Today 190 (2012) 107–111.
[54] A. Goyal, S. Bansal, S. Singhal, Int. J. Hydrogen Energy 39 (2014) 4895–4908.
[55] D.Z. Jiang, J. Xie, D. Jiang, X. Wei, M. Chen, CrystEngComm 15 (2013) 560–569.
[56] Y.-G. Wu, M. Wen, Q.-S. Wu, H. Fang, J. Phys. Chem. C 118 (2014) 6307–6313.
[57] R. Xu, H. Bi, G. He, J. Zhu, H. Chen, Mater. Res. Bull. 57 (2014) 190–196.
[58] Z. Wang, C. Xu, G. Gao, X. Li, RSC Adv. 4 (2014) 13644–13651.
[59] B.J. Borah, P. Barali, J. Mol. Catal. A Chem. 390 (2014) 29–36.
[60] K.-L. Wu, X.-W. Wei, X.-M. Zhou, D.-H. Wu, X.-W. Liu, Y. Ye, Q. Wang, J. Phys. Chem. C 115 (2011) 16268–16274.
[61] K.-L. Wu, R. Yu, X.-W. Wei, CrystEngComm 14 (2012) 7626–7632.
[62] S. Li, S. Guo, H. Yang, G. Gou, R. Ren, J. Li, Z. Dong, J. Jin, J. Ma, J. Hazard. Mater. 270 (2014) 11–17.
[63] X. Chen, Z. Cai, X. Chen, M. Oyamac, J. Mater. Chem. A 2 (2014) 5668–5674.
[64] B. Sreedhar, D.K. Devi, D. Yada, Catal. Commun. 12 (2011) 1009–1014.
[65] Z. Wang, C. Xu, G. Gao, X. Li, RSC Adv. 4 (2014) 13644–13651.
[66] X. Wang, J. Fu, M. Wang, Y. Wang, Z. Chen, J. Zhang, J. Chen, Q. Xu, J. Mater. Sci. 49 (2014) 5056–5065.
[67] R.J. Kalbasi, A.A. Nourbakhsh, F. Babaknezhad, Catal. Commun. 12 (2011) 955–960.
[68] C. Xu, Y. Yuan, R. Yuan, X. Fu, RSC Adv. 3 (2013) 18002–18008.
[69] M. Xie, F. Zhang, Y. Long, J. Ma, RSC Adv. 3 (2013) 10329–10334.
[70] Z. Duan, G. Ma, W. Zhang, Bull. Korean Chem. Soc. 33 (2012) 4003–4006.
[71] P. Wang, F. Zhang, Y. Long, M. Xie, R. Li, J. Ma, Catal. Sci. Technol. 3 (2013) 1618–1624.
[72] N. Sahiner, H. Ozay, O. Ozay, N. Aktas, Appl. Catal. A Gen. 385 (2010) 201–207.
[73] A.K. Shil, D. Sharma, N.R. Guha, P. Das, Tetrahedron Lett. 53 (2012) 4858–4861.
[74] H. Yang, S. Li, X. Zhang, X. Wang, J. Ma, J. Mater. Chem. A 2 (2014) 12060–12067.
[75] Z. Dong, X. Le, X. Li, W. Zhang, C. Dong, J. Ma, Appl. Catal. B Environ. 158–159 (2014) 129–135.
[76] D. Shah, H. Kaur, J. Mol. Catal. A Chem. 381 (2014) 70–76.
[77] K. Layek, M.L. Kantam, M. Shirai, D. Nishio-Hamane, T. Sasaki, H. Maheswaran, Green Chem. 14 (2012) 3164–3174.
[78] M. Islam, P. Mondal, A.S. Roy, K. Tuhina, Trans. Met. Chem. 35 (2010) 427–435.
[79] Y. Choi, H.S. Bae, E. Seo, S. Jang, K.H. Park, B.-S. Kim, J. Mater. Chem. 21 (2011) 15431–15436.
[80] J. Li, C.-Y. Liu, Y. Liu, J. Mater. Chem. 22 (2012) 8426–8430.
[81] Z. Wang, C. Xu, G. Gao, X. Li, RSC Adv. 4 (2014) 13644–13651.
[82] N. Sahiner, Prog. Polym. Sci. 38 (2013) 1329–1335.
[83] M. Nasrollahzadeh, S.M. Sajadi, A. Rostami-Vartooni, M. Bagherzadeh, R. Safari, J. Mol. Catal. A Chem. 400 (2015), 22–0.
[84] Y. Zhang, P. Zhu, L. Chen, G. Li, F. Zhou, D. Lu, R. Sun, F. Zhou, C.-p. Wong, J. Mater. Chem. A 2 (2014) 11966–11973.
[85] X. Yang, H. Zhong, Y. Zhu, H. Jiang, J. Shen, J. Huang, C. Li, J. Mater. Chem. A 2 (2014) 9040–9047.
[86] Z. Gan, A. Zhao, M. Zhang, W. Tao, H. Guo, Q. Gao, R. Mao, E. Liu, Dalton Trans. 42 (2013) 8597–8605.
[87] Z.J. Jiang, C.Y. Liu, L.W. Sun, J. Phys. Chem. B 109 (2005) 1730–1735.
[88] S. Dutt, P.F. Siril, V. Sharma, S. Periasamy, N. J. Chem. 39 (2015) 902–908.
[89] P. Zhang, Y. Sui, C. Wang, Y. Wang, G. Cui, C. Wang, B. Liu, B. Zou, Nanoscale 6 (2014) 5343–5354.
[90] S. Xuan, Y.X.J. Wang, J.C. Yu, K.C.F. Leung, Langmuir 25 (19) (2009) 11835–11843.
[91] B. Zhang, B. Zhao, S. Huang, R. Zhang, P. Xu, H.L. Wang, CrystEngComm 14 (2012) 1542–1544.
[92] L. Ai, C. Zeng, Q. Wang, Catal. Commun. 14 (2011) 68–73.
[93] Z.-J. Jiang, C.-Y. Liu, L.-W. Sun, J. Phys. Chem. B 109 (2005) 1730–1735.
[94] Z. Deng, H. Zhu, B. Peng, H. Chen, Y. Sun, X. Gang, P. Jin, J. Wang, ACS Appl. Mater. Interfaces 4 (2012) 5625–5632.
[95] B.K. Ghosh, S. Hazra, B. Nak, N.N. Ghosh, Powder Technol. 269 (2015) 371–378.